

LIBRAHY ∕lichigan State University

This is to certify that the thesis entitled

MECHANICAL DOMAIN PARAMETRIC AMPLIFICATION IN MULTI-DEGREE-OF-FREEDOM SYSTEMS

presented by

Nicholas J. Miller

has been accepted towards fulfillment of the requirements for the

M.S. degree in Mechanical Engineering

Major Professor's Signature

12/10/167

Date

MSU is an affirmative-action, equal-opportunity employer

PLACE IN RETURN BOX to remove this checkout from your record.

TO AVOID FINES return on or before date due.

MAY BE RECALLED with earlier due date if requested.

DATE DUE	DATE DUE	DATE DUE

5/08 K:/Proj/Acc&Pres/CIRC/DateDue indd

MECHANICAL DOMAIN PARAMETRIC AMPLIFICATION IN MULTI-DEGREE-OF-FREEDOM SYSTEMS

By

Nicholas J. Miller

A THESIS

Submitted to
Michigan State University
in partial fulfillment of the requirements
for the degree of

Master of Science

Department of Mechanical Engineering

2007

ABSTRACT

MECHANICAL DOMAIN PARAMETRIC AMPLIFICATION IN MULTI-DEGREE-OF-FREEDOM SYSTEMS

By

Nicholas J. Miller

Parametric amplification, or amplification of an oscillator's resonance by periodic variations in its parameters, can exist in both degenerate and nondegenerate forms in multi-degree-of-freedom mechanical systems. In particular, micro-electro-mechanical systems are prime for parametric amplification since common forms of electrostatic forcing produce parametric effects. In this thesis we demonstrate degenerate parametric amplification in a macro-scale mechanical system, and discuss the application of both degenerate and nondegenerate amplification in multi-degree-of-freedom systems. We present a formulation of expressions for parametric amplification of primary and combination resonances of multiple-degree-of-freedom systems. We also show that for systems with appropriate frequency separation, degenerate parametric amplification can be used to produce resonance quality enhancement during frequency sweeps, thus allowing us to enhance the resonance quality observed during a sweep without prior knowledge of resonance location. This technique is applied to a multi-degree-of-freedom chemical mass sensor. Simulations are presented. We also show that under proper excitation conditions, parametric excitation can be used to transfer energy between system modes, but this effect is dependent on the phase between the forcing on the participating modes. The results show that with proper conditions, including phase, it is possible to suppress the vibration amplitude of a forced mode to $O(\epsilon)$, by effectively transferring the forcing to another mode.

To my parents

ACKNOWLEDGMENTS

This work would not have been possible without the efforts of my advisor, Dr. Steve Shaw. I would also like to thank Dr. Jeff Rhoads, and Drs. Brian Feeny, Cevat Gokcek, and Alan Haddow.

This material is based on work supported by the National Science Foundation under grants No. ECCS-0428916 and CMMI-0408866. Any opinions, findings, conclusions or recommendations expressed in this material are those of the authors and do not necessarily reflect the views of the National Science Foundation.

TABLE OF CONTENTS

LI	ST C	OF TABLES	vi
LI	ST C	OF FIGURES	vi
1	Int	roduction	1
	1.1	Parametric Excitation, Amplification, and Resonance	1
	1.2	A Brief History	4
	1.3	Current Interest in Parametric Amplification	6
	1.4	Methods of Implementation in Mechanical Systems	7
	1.5	Outline	9
2	Bac	kground: Analysis of Parametric Amplification	11
	2.1	Degenerate Amplification	11
		2.1.1 Modeling	12
		2.1.2 Analysis	16
		2.1.3 Experimental Results	20
	2.2	The Manley-Rowe Equations	22
	2.3		24
3			31
		Analysis	31
	3.2	Parametrically Amplified Frequency Sweeping: An Application	
		Illustrated by Example	39
		3.2.1 Numeric Analysis	4 2
4	Cor	aclusions and Future Work	55
AJ	PPE	NDICES	57
A	Mu	ltiple Scales Analysis	57
	A.1	Case 1: Near an isolated primary resonance, $\Omega pprox \omega_{\pmb{k}}$	5 8
	A.2	Case 2: Near an isolated resonance of the sum type, $\Omega \approx \omega_p + \omega_q$	60
	A.3	Case 3: Near an isolated resonance of the difference type, $\hat{\Omega} \approx 1$	
		$\omega_q - \omega_p$	6 3
	A.4		63
	A.5	Case 5: Near $\omega_q - \omega_p$ and $\omega_s - \omega_q$	66
RI	RI.I	OGRAPHY	R 9

LIST OF TABLES

2.1	SCALING SUBSTITUTIONS	15
2.2	Nondimensional parameter definitions. Note that $arepsilon$ respresents	
	a 'small' parameter introduced for analytical purposes and ω rep-	
	resents the system's 'physical' base excitation frequency	17

LIST OF FIGURES

2.1	Experimental setup [1]	12
2.2	Schematic of base-excited cantilever [1]	13
2.3	Wedge of instability near $\sigma=0$. Note that parametric amplification requires that the operating point be below the wedge, as parametric resonance occurs above [1]	19
2.4	Frequency response for three parametric pump amplitudes [1]. The continuous lines indicate theoretical results, the points indicate measured data	21
2.5	Time lapse photographs [1]	22
2.6	Gain vs normalized pump amplitude [1]. The pump amplitude is normalized such that $\lambda_{2,crit}=1$. The continuous line indicates theoretical result, the points indicate measured data	23
2.7	Gain vs phase [1]. The continuous line indicates theoretical results, the points indicate measured data	24
2.8	Wedges of instability for the non-degenerate resonator, for $\omega_s=1$, $\omega_i=1.5$, $\zeta_s=0.01$, $\zeta_i=0.01$, $\gamma=1$, $\epsilon=1$	27
2.9	Gain of the non-degenerate resonator, for $\omega_s=1,\omega_i=1.5,$ $\zeta_s=0.01,\zeta_i=0.01,\gamma=1,\epsilon=1$	29
3.1	Gain curves for multiple scales solution, case 1	35
3.2	An SEM of the SISO device [2]	43
3.3	Lumped mass model of SISO device [2]	43
3.4	Frequency response. a) Magnitude, b) Phase [2]	44
3.5	Experimental frequency response taken at 6.2 V AC in 275mTorr pressure [2]	45
3.6	SEM image of platinum patch [2]	46
3.7	Experimental frequency response taken at 12.2 V AC in 275mTorr pressure [2]	47
3.8	Experimental frequency response near resonance D [2]	47

3.9	Experimental frequency response near resonance C [2]	48
3.10	Bode plot for SISO model used for simulation	48
3.11	Close up of beam resonances	49
3.12	Stability boundary. Gray regions are unstable, white regions are stable	51
3. 13	Stability boundary around beam frequencies. Gray regions are unstable, white regions are stable	51
3.14	Pump value vs. frequency for multiple scales solution. Shown against stability boundary. Again, gray regions are unstable, and white regions are stable	53
3.15	Numerical simulation of the pumped system	53
3.16	Close up of the first resonance for the numerical simulation of the pumped system	54

CHAPTER 1

Introduction

1.1 Parametric Excitation, Amplification, and Resonance

In this thesis we discuss parametric amplification in mechanical systems. By parametric amplification, we mean the increase in energy of a resonator by a periodic variation of the parameters of that resonator. If we view the variation in a parameter as an input, or applied signal, we can say that we are exciting or forcing the system parametrically, or through its parameters. This we term parametric excitation. Parametric amplification, to reiterate our statement above, is the amplification of a resonator's response as a result of parametric excitation. In a simple RLC circuit, for example, the resistance, capacitance, and inductance may be varied to produce an amplified output. In a mechanical device, the mass, damping coefficient, and stiffness may be varied. A parametric amplifier, however, cannot produce power gain if the only time varying component is a locally passive resistance or damping coefficient [3]. Typically, it is only the capacitance in electrical circuits and stiffness in mechanical devices that are parametrically pumped.

In order to illustrate this principle, consider the example of a simple mechanical resonator, say a cantilevered beam which is experiencing a small force at its fundamental resonant frequency. The beam will vibrate in response with

an amplitude proportional to the magnitude of the force, and the total energy of the beam will settle at a constant value. Now, imagine that the stiffness of the beam begins to vary with time in the following way. When the beam reaches its peak deflection, let the stiffness of the beam be suddenly increased above the nominal value. This sudden increase in stiffness corresponds to a sudden increase in potential energy. The potential energy is subsequently converted into kinetic energy as the beam is pulled back to its center position. As it crosses the centerline, let the stiffness be suddenly reduced to its original value. This reduction in stiffness occurs without detriment to the system's energy because there is no potential energy when the beam deflection is zero, i.e., all the beam's energy is stored as kinetic energy at that time. Let this cycle continue, and it is plain to see that this variation in stiffness effectively 'pumps' energy into the beam. The total energy will continue to increase, as well as the amplitude of oscillation, until the effect saturates due to either increasing dissipation, or nonlinear effects. It is important to note that the variation in stiffness is periodic with a period half that of the beam motion, yet it increases the resonator motion at its fundamental frequency. As Mumford wrote, "This principle may be broadly stated thus: The energy of an oscillating system may be increased by supplying energy at a frequency which differs from the fundamental frequency of the oscillator" [4].

The above example is an illustration of a so-called degenerate parametric amplification. In this specific case, the pump frequency is twice that of the resonator. In the general degenerate case, however, energy can be pumped into a single resonator at its fundamental frequency, from the family of frequencies, $\omega_p = \frac{2\omega_S}{n}$, where ω_S is the resonator's fundamental frequency, also known as the signal frequency, and n is a nonzero positive integer, n=1,2...

It is also important to note the phase of the parametric variation. In the

example above, the parametric variation is in phase with the beam motion. If, on the other hand it were out of phase by 90 degrees, the stiffness would increase as the beam crosses the centerline, and thus result in no change in energy. Meanwhile, the stiffness would decrease as the beam reaches its peak, causing a decrease in the potential energy. The effect is not an increase in energy, but a decrease of the beam's energy, and therefore attenuation of the motion.

The non-degenerate species of parametric amplification is a bit more complex, and so we will not attempt to illustrate it with a thought experiment here. As far as general introductions are concerned, suffice it to say that non-degenerate amplification does not have a phase dependence between the pump and the resonator. Nor does it require the same frequency relationship between the pump frequency and the resonator's fundamental frequency. Non-degenerate amplification does, however, require multiple parametrically coupled resonators. By parametrically coupled, we mean coupled with timevarying parameters. This mode of parametric amplification is best explained by example of its most common manifestation, the three-frequency amplifier. Herein two resonators are parametrically coupled. One of the two resonators is directly forced, and the other is not. This setup is called a three-frequency amplifier because, not surprisingly, it has three frequencies. The forced resonator's fundamental frequency (or signal frequency) is termed ω_s , the pump frequency, ω_p , and the unforced resonator frequency, or idler, resonator, ω_i . The frequency condition for three-frequency non-degenerate amplification is $\omega_i = (\omega_s + r\omega_p)$, where r is an integer, typically taken to be -1. Both degenerate and non-degenerate parametric amplification are are thoroughly treated in [5, 3, 6]. Degenerate amplification is demonstrated in a mechanical system in [7], among others, and non-degenerate amplification is demonstrated in a

mechanical system in [8].

Above, we briefly glossed over the notion that the amplified response could be saturated by nonlinearities in the system. We recall this here to make one last note before moving forward with our discussion of parametric amplification. Parametric amplification is a linear, frequency specific, signal amplification technique. Accordingly, in this thesis, we consider only linear system models, limiting our analysis to below the threshold where parametric pumping destabilized the zero solution. Beyond this threshold lies parametric resonance, the situation where the parametric excitation alone, i.e., without any direct excitation, causes the resonator to oscillate. In linear investigations of parametrically excited systems the threshold between parametric amplification and parametric resonance manifests itself as a singularity, in the amplification or gain induced by parametric pumping. At this singularity the linear equations predict infinite gain which is, of course, not possible. Accordingly, when we encounter this singularity in our analysis we will simply regard it as the boundary where our solution fails. For further discussion of parametric resonance, we refer the reader to [9].

1.2 A Brief History

The most commonplace example of parametric excitation is probably a child's swing, wherein the child pumps the swing's oscillation by varying the position of his or her center of mass. This idea must be very old indeed, but with regard to the science and engineering community, the first observation of this phenomenon is attributed to Faraday in 1831 [4]. Faraday observed parametric effects in waves upon a surface of water. In 1859 Melde performed an experiment wherein he tied a tuning fork to a fine string, the motion of the tuning fork being parallel to the length of the string. The vibration of the tuning fork varied

	,			
		·		
•				

the tension in the string, and thus its stiffness, causing sustained transverse vibrations in the string at half the frequency of the tuning fork [4]. Strictly speaking, these examples are not of parametric amplification, but parametric resonance.

Analogous experiments to those of Faraday and Melde were carried out with electrical circuits, eventually leading to a successful parametric amplifier attributed to Alexanderson. This device used variable inductance, and was used in radio telephones [10]. In the mid 20th century the variable capacitor, or varactor, was created, and proved to have much better noise properties than variable inductance elements [5].

Noise issues are in fact one of the big motivators for parametric amplification. In 1957, Heffner and Wade were the first to consider the theoretical noise, gain, and bandwidth properties [4]. The noise properties were, however, more dramatically summed up by Caves. In his work on noise in linear amplifiers, he states "an ideal degenerate paramp [parametric amplifier] is noiseless" [11]. In 1958 the theoretical low-noise properties were experimentally verified at the Bell Telephone Laboratories by Engelbrecht [4]. Real parametric amplifiers are, of course, non-ideal, so Caves's statement is not possible to realize. Nevertheless, they do not suffer from Johnson, Shot, or 1/f noise because they are not based on semiconductor junction effects and resistors [12]. This results in low-noise amplifiers. Despite these favorable low-noise properties, parametric amplifiers could not compete with Metal-Semiconductor Field Effect Transistors, or MESFETs, for microwave applications [12], and were subsequently abandoned.

While parametric amplifiers are no longer commonly used in microwave applications, parametric amplification has certainly found a new home in optical and micro-mechanical systems. In fact, it could be argued that parametric

amplification persists as a part of a general vibrational control theory which utilizes parametric excitation, which is potential applicable to a wide variety of systems. This type of vibrational control uses high frequency, zero mean, parameter variation in order to change the locations of the averaged poles of a plant system [13, 14]. This is done without feedback or disturbance measurement, but has the potential to both stabilize the plant and reject disturbances. Certainly, parametric resonance amplification could be viewed as the act of moving the poles of the averaged system closer to the imaginary axis, thus reducing the effects of dissipation and increasing resonance quality. This specific technique, parametric amplification, rather than the general technique of vibrational control, has become of interest in a variety of areas lately because the effect is often either inherent, or can be easily designed into a system to increase performance.

1.3 Current Interest in Parametric Amplification

Parametric Amplification currently has possible applications in electrical, mechanical, optical, thermal, and acoustic areas. Generally, the interest is in sensor applications because the low noise properties of parametric amplifiers offer the possibility of very clean sensor signals. Parametric effects have been utilized in thermal IR sensors [15], and acoustic parametric amplification has been shown using bulk acoustic waves (BAWs) [16]. Optical parametric amplification is used to amplify small signals in lasers [17]. In the electrical field, parametric amplifiers have gained renewed interest in application to Josephson junction arrays [18].

Mechanical parametric amplification finds its major outlet in MEMs application, beginning with the seminal work by Rugar and Grütter [7], wherein electrostatic forcing was used to parametrically amplify the oscillation of a can,

tilevered beam. Rugar and Grütter employed degenerate parametric amplification and demonstated its phase dependant gain and noise-squeezing properties. Following this line, parametric excitation has been employed in MEMsbased parametric amplifiers and filters [12, 19]. Some of the benefits of MEMsbased amplifiers include the ability to operate in environments where CMOS technology fails. High temperature environments such as combustion chambers, and particle bombardment environments such as nuclear reactors are some examples [12]. Other mechanical applications include electric force microscopy [20], atomic force microscopy [7, 21], and magnetic resonance force microscopy [22]. Kaajakari and Lal use parametric excitation in a microactuator, inducing torsional displacement in a micro rotor [23]. Currently there is also a great deal of interest in the rich dynamics of large systems of parametrically coupled resonators [24, 25, 26]. There is also significant effort to employ parametric amplification to boost the quality factor of resonators used in MEMs sensors [22, 27]. This will be the focus of chapter 3, where modal Qenhancement by parametric amplification in multi-degree-of-freedom systems will be considered.

1.4 Methods of Implementation in Mechanical Systems

Parametric amplification requires the periodic variation of some parameters of the resonator who's response is being amplified. There is certainly some flexibility in the choice of parameter variation, though in mechanical systems stiffness is nearly universally chosen. The methods of stiffness variation, however, are quite diverse.

Rugar and Grütter used the nonlinearity of electrostatic forcing to produce parametric effects. When the resonator amplitude is of sufficient magnitude that the first two terms of the Taylor series are contributary, the nonlinear electrostatic force modulates the cantilever stiffness. This approach is common, and is used in [7, 12, 28, 29].

Another common source of parametric excitation is base excitation, as in the classical base excited pendulum. Here the reaction forces induced by the acceleration of the base creates a time varying stiffness. This method was used by the author and others with a fixed-free beam in [1], and is demonstrated here in section 2.1.

Lorentz forces are used on a cantilever in [30]. Here, a magnetic field is coupled to a current at the tip of the cantilever running perpendicular to the longitudinal direction. This creates an axial force on the cantilever which modifies the transverse stiffness of the cantilever. The current can then be easily utilized to modulate the stiffness creating parametric amplification or resonance.

Quadratic nonlinear stiffness is employed in [21]. The quadratic nonlinearity creates a modulated stiffness with frequency twice that of the direct excitation, thus producing a degenerate parametric effect. The quadratic stiffness is generated by the curved geometry of the region that connects the cantilever to the base.

Local heating induced by a low-power laser beam is used on silicon disk resonators in [31]. The local heating at the periphery of the disk causes a significant change in the effective stiffness. Modulating the laser in this way yields parametric effects.

Roukes accomplishes parametric amplification of a nano scale fixed-fixed beam by applying an axial load through the beam supports[32]. This methos is in the same vein as Melde's string and tuning fork experiment. In both cases the axial force modifies the stiffness of the resonator, thus parametrically pumping transverse vibrations.

Centrifugal forcing of transversely vibrating cantilevered beams can also exhibit parametric effects. The centrifugal force can be used to either harden or soften the beam's intrinsic stiffness in a time varying manner.

1.5 Outline

The remainder of this thesis is organized in the following way. Chapter 2 presents the background material. Degenerate parametric amplification of a single degree of freedom system is presented. In addition, we present an experiment wherein parametric amplification is demonstrated on a macroscale cantilevered beam. The Manley-Rowe equations are presented. These equations describe the average power relationships between resonances under parametric amplification, and respresent the pre-existing general solution to parametric amplification in multi-degree-of-freedom systems. Nondegenerate amplification is also presented in the context of the three-frequency amplifier. In chapter 3, we consider parametric amplification of multi-degree-of-freedom systems. Here we develop an expression that describe the vibration behavior of such a system under both direct and parametric excitation. This is done using perturbation techniques. This analysis is accompanied by a numerical example where we employ parametric amplification to provide resonance quality enhancement to frequency sweeps in a resonant multi-degree-of-freedom chemical mass sensor. This device was presented by DeMartini et al. in [2]. Finally, in chapter 4, conclusions and a discussion of possible future work are presented.

The major contributions of this work include the formulation of O(1) expressions for parametric amplification of primary and combination resonances of multiple-degree-of-freedom systems. These expressions give more specific descriptions of the device behavior than the Manley-Rowe equations. Specif-

ically, these expressions provide amplitude, phase, gain, stability, and local frequency response information. The Manley-Rowe equations, on the other hand, provide only the average power transfered to the resonators from the parametric pump. In addition, we demonstrate that systems with appropriate frequency conditions allow parametric amplification to be piggy-backed on frequency sweeps, thus allowing us to enhance the resonance quality observed during a sweep without prior knowledge of resonance location. We also show that under proper excitation conditions, parametric excitation can be used to transfer energy between system modes, but this effect is dependent on the phase between the forcing on the participating modes. This effect is not captured by Manley-Rowe. This result shows that with proper conditions, including phase, it is possible to suppress the vibration amplitude of a forced mode to $O(\epsilon)$.

CHAPTER 2

Background: Analysis of Parametric Amplification

In the introduction we presented an intuitive explanation of degenerate parametric amplification. Here, we explore both degenerate and nondegenerate amplification from an analytical perspective. Both cases, that is degenerate and non-degenerate, will be encountered in the application of this technique to multi-degree-of-freedom systems discussed in chapter 3. In this chapter we begin with degenerate parametric amplification in section 2.1. Degenerate amplification is presented in the context of an experiment done in cooperation with Rhoads et al., and presented in [1]. As such, the discussion of amplification is preceded by a short discussion of modeling, wherein the source of the parametric excitation is shown. In section 2.2, the Manley-Rowe equations are presented as preliminary results to the discussion of nondegenerate parametric amplification, which follows in section 2.3. Non-degenerate parametric amplification is presented in its most common form, the three-frequency amplifier.

2.1 Degenerate Amplification

As we are illustrating degenerate parametric amplification by example, we begin our discussion with a detour into system modeling. We consider a fixed-free



Figure 2.1. Experimental setup [1].

cantilever beam subject to base excitation in both the transverse and the longitudinal directions. This model development was first presented in [1], and is reproduced here with permission of the authors. As we will see in 2.1.1, this longitudinal base excitation produces parametric effects. Analysis of degenerate parametric amplification is presented in 2.1.2. The results of the analysis are presented alongside the results of the experiment in 2.1.3.

2.1.1 Modeling

Now, consider the fixed-free beam shown in figure 2.1. The beam is a spring steel beam, clamped at one end to the excitation table of a vibration exciter. The beam is oriented vertically, while the exciter is oriented at an angle $\alpha =$

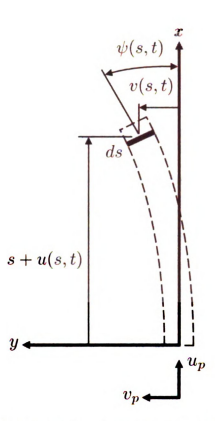


Figure 2.2. Schematic of base-excited cantilever [1].

 80° . This provides both longitudinal and transverse base motion, the relative magnitudes of which depend on α . A schematic representation of the system is shown in figure 2.2.

The Lagrangian for the this system can be approximated by

$$\bar{L} = \frac{1}{2}\rho A \left[(\dot{u} + \dot{u}_p)^2 + (\dot{v} + \dot{v}_p)^2 \right] - \frac{1}{2}EI(\psi')^2, \tag{2.1}$$

where u,v, and ψ are defined in the figure. (\bullet) and $(\bullet)'$ represent time and space derivatives with respect to time, t, and arc length, s. u_p and v_p specify the imposed base motion in the longitudinal and transverse directions. ρ , A, E, and I represent the beam's density, cross-sectional area, modulus of elasticity, and cross-sectional moment of inertia, respectively. Applying the extended

· :		

Hamilton's principle with an imposed inextensibility constraint gives

$$\delta H = \delta \int_{t_1}^{t_2} \int_0^l \left\{ \bar{L} + \frac{1}{2} \lambda \left[1 - \left(1 + u' \right)^2 - (v')^2 \right] \right\} ds dt + \int_{t_1}^{t_2} \int_0^l \left(Q_u \delta u + Q_v \delta v \right) ds dt,$$
(2.2)

where l is the beam's undeformed length, λ is the Lagrange multiplier used to impose the inextensibility constraint, and Q_u and Q_v represent u and v components of the non-conservative forces and conservative forces that are not included in the potential energy formulation. Assuming that damping only has appreciable effects on the transverse motion, these forces can be approximated by

$$Q_u = -\rho Ag, \qquad Q_v = -c\dot{v}, \tag{2.3}$$

where g is the acceleration due to gravity, and c is the viscous damping coefficient. Applying the kinematic constraint

$$\tan(\psi) = \frac{v'}{1+u'} \tag{2.4}$$

and the extended Hamilton's principle gives the partial differential equations

$$\rho A\ddot{v} + c\dot{v} + EIv^{iv} - v''\rho A\ddot{u}_p(s-l) - v'\rho A\ddot{u}_p$$

$$- v''\rho Aq(s-l) - v'\rho Aq = -\rho a\ddot{v}_p.$$
(2.5)

To reduce the number of free parameters, it is convenient to rescale this equation by the substitutions enumerated in table 2.1, where v_0 is some additional characteristic length, e.g. the width or thickness of the beam. The reduced distributed parameter model is given by

$$\ddot{\hat{v}} + \hat{c}\dot{\hat{v}} + \hat{v}^{iv} - \frac{v_0}{l}\ddot{\hat{u}}_p(\hat{s} - 1)\hat{v}'' - \frac{v_0}{l}\ddot{\hat{u}}_p\hat{v}' - \frac{\rho Agl^3}{EI}(\hat{s} - 1)\hat{v}'' - \frac{\rho Agl^3}{EI}\hat{v}' = -\ddot{\hat{v}}_p,$$
(2.6)

Table 2.1. SCALING SUBSTITUTIONS

$$\hat{s} = \frac{s}{l} \qquad \hat{t} = \frac{t}{T} \qquad T = \sqrt{\frac{\rho A l^4}{ET}}$$

$$\hat{v} = \frac{v}{v_0}, \qquad \hat{u}_p = \frac{v_p}{v_0}, \qquad \hat{v}_p = \frac{v_p}{v_0} \qquad \hat{c} = \frac{cT}{\rho A}$$

Here, the time and length derivatives have been redefined in terms of new time and length variables, \hat{t} and \hat{s} . Since the frequencies of excitation are near the beams first natural frequency, and twice that, and yet both are still significantly below the beam's second natural frequency, we simplify the system still further by ignoring all but the first mode. Accordingly we use a Galerkin projection to reduce (2.6) to a lumped parameter model by assuming a separable solution and projecting equation (2.6) onto the first mode shape. Thus, we let

$$\hat{v} = z(\hat{t})\Phi(\hat{s}),\tag{2.7}$$

where Φ is normalized such that $\int_0^1 \Phi^2 d\hat{s} = 1$. And so, equation (2.6) becomes

$$\ddot{z}\Phi + \hat{c}\dot{z}\Phi + z\Phi^{iv} - \frac{v_0}{l}\ddot{\hat{u}}_p(\hat{s} - 1)z\Phi'' - \frac{v_0}{l}\ddot{\hat{u}}_pz\Phi'
- \frac{\rho Agl^3}{EI}(\hat{s} - 1)z\Phi'' - \frac{\rho Agl^3}{EI}z\Phi' = -\ddot{\hat{v}}_p,$$
(2.8)

We then take the inner product of this equation with the assumed mode shape, Φ .

$$\ddot{z} \int_{0}^{1} \Phi^{2} d\hat{s} + \hat{c}\dot{z} \int_{0}^{1} \Phi^{2} d\hat{s} + z \int_{0}^{1} \Phi \Phi^{iv} d\hat{s} - \frac{v_{0}}{l} \ddot{u}_{p} z \int_{0}^{1} (\hat{s} - 1) \Phi \Phi'' + \Phi \Phi' d\hat{s}$$

$$- \frac{\rho A g l^{3}}{E I} z \int_{0}^{1} (\hat{s} - 1) \Phi \Phi'' + \Phi \Phi' d\hat{s} = -\ddot{v}_{p} \int_{0}^{1} \Phi d\hat{s},$$
(2.9)

Here we also choose a specific form for the base motion,

$$\hat{u}_p = \hat{x}_p \sin(\alpha), \qquad \hat{v}_p = \hat{x}_p \cos(\alpha),$$
 (2.10)

$$\hat{x}_p = \hat{A}\cos(\hat{\omega}\hat{t} + \phi) + \hat{B}\cos(2\hat{\omega}\hat{t}), \tag{2.11}$$

and, the final lumped-parameter model is

$$z'' + 2\varepsilon\zeta z' + z + \left[\varepsilon\lambda_1\Omega^2\cos(\Omega\tau + \phi) + \varepsilon\lambda_2\Omega^2\cos(2\Omega\tau)\right]z$$

$$= \varepsilon\eta_1\Omega^2\cos(\Omega\tau + \phi) + \varepsilon\eta_2\Omega^2\cos(2\Omega\tau),$$
(2.12)

with parameters defined in table 2.2. From equations (2.10) and (2.11), and table 2.2, we can see that the longitudinal component of the base motion, \hat{u}_p , is responsible for the parametric excitation via λ_1 and λ_2 . Similarly, the transverse component of the base motion, \hat{v}_p , is responsible for the direct excitation via η_1 and η_2 .

2.1.2 Analysis

The time-vary nature of equation (2.12) prevents a tractable closed-form solution, and so the method of averaging [33] is used to give an approximate solution. Parametric amplification is a resonant effect, so we assume the frequency condition

$$\Omega = 1 + \varepsilon \sigma. \tag{2.13}$$

In addition, we expect that the steady state response will be near the frequency of the resonant direct excitation term. This motivates the constrained coordinate change

$$z(\tau) = X(\tau)\cos(\Omega\tau) + Y(\tau)\sin(\Omega\tau),$$

$$z'(\tau) = -X(\tau)\Omega\sin(\Omega\tau) + Y(\tau)\Omega\cos(\Omega\tau).$$
(2.14)

Table 2.2. Nondimensional parameter definitions. Note that ε respresents a 'small' parameter introduced for analytical purposes and ω represents the system's 'physical' base excitation frequency.

$$\tau = \omega_0 \hat{t}, \qquad (\bullet)' = \frac{d(\bullet)}{d\tau}$$

$$\hat{\omega} = \omega T, \qquad \Omega = \frac{\hat{\omega}}{\omega_0}$$

$$\omega_0^2 = \int_0^1 \Phi \Phi^{iv} d\hat{s} - \frac{\rho A l^3 g}{EI} \left(\int_0^1 \Phi \Phi''(\hat{s} - 1) d\hat{s} + \int_0^1 \Phi \Phi' d\hat{s} \right)$$

$$\varepsilon \zeta = \frac{\hat{c}}{2\omega_0}$$

$$\varepsilon \lambda_1 = \frac{\hat{A} v_0 \sin \alpha}{l} \left(\int_0^1 \Phi \Phi''(\hat{s} - 1) d\hat{s} + \int_0^1 \Phi \Phi' d\hat{s} \right)$$

$$\varepsilon \lambda_2 = \frac{4 \hat{B} v_0 \sin \alpha}{l} \left(\int_0^1 \Phi \Phi''(\hat{s} - 1) d\hat{s} + \int_0^1 \Phi \Phi' d\hat{s} \right)$$

$$\varepsilon \eta_1 = \hat{A} \cos(\alpha) \int_0^1 \Phi d\hat{s}, \qquad \varepsilon \eta_2 = 4 \hat{B} \cos(\alpha) \int_0^1 \Phi d\hat{s}$$

Subsequently, the method of averaging gives the following equations

$$X' = -\frac{1}{4}\varepsilon \left(\lambda_2 Y + 4\sigma Y + 4\zeta X - 2\eta_1 \sin \phi\right),$$

$$Y' = -\frac{1}{4}\varepsilon \left(\lambda_2 X - 4\sigma X + 4\zeta Y - 2\eta_1 \cos \phi\right).$$
(2.15)

The steady state solutions of equations (2.15) give the steady state solutions to equation (2.12) by use of equation (2.14). We find that the system has a steady state solution with amplitude and phase given by

$$\bar{a} = \sqrt{X^2 + Y^2}$$

$$= 2\sqrt{\frac{\eta_1^2 \left[\lambda_2^2 + 16(\zeta^2 + \sigma^2) + 8\lambda_2 \left(\sigma \cos 2\phi - \zeta \sin 2\phi\right)\right]}{\left[\lambda_2^2 - 16(\sigma^2 + \zeta^2)\right]^2}}, (2.16)$$

.

$$\bar{\psi} = \arctan\left[\frac{Y}{X}\right] = \arctan\left[\frac{(\lambda_2 - 4\sigma)\sin\phi - 4\zeta\cos\phi}{(\lambda_2 + 4\sigma)\cos\phi - 4\zeta\sin\phi}\right].$$
 (2.17)

Defining gain as

$$G = \frac{\bar{a}_{pump\ on}}{\bar{a}_{pump\ of\ f}},\tag{2.18}$$

the gain at resonance, ($\sigma = 0$), is given by

$$G(\sigma = 0) = 4\zeta \sqrt{\frac{\lambda_2^2 + 16\zeta^2 - 8\lambda_2\zeta\sin 2\phi}{(\lambda_2^2 - 16\zeta^2)^2}}.$$
 (2.19)

The gain expression, equation (2.19), is only valid for the range of parameters where equations (2.15) have a stable fixed point. This parameter space is defined by $\lambda_2 < \lambda_{2,crit}$,

$$\lambda_{2,crit} = 4\sqrt{\sigma^2 + \zeta^2}. (2.20)$$

The λ_2 threshold also coincides with the singularities in the amplitude and gain equations, equations (2.16) and (2.19). Figure 2.3 shows $\lambda_{2,crit}$ in the σ , λ_2 plane around the area of operation. $\lambda_{2,crit}$ is shown for various values of ζ . These curves are the so-called wedges of instability, which divide the stable parameter space (below the wedges), from the unstable parameter space (above the wedges). Above the wedges the real device will enter parametric resonance, a phenomenon that is not captured by the linear model used here.

In addition to the amplitude and gain formulas presented here, we can also develop an expression for the quality factor of a resonator under degenerate parametric amplification. This is done by looking for the detuning value, (σ) , where the amplitude, equation (2.16), is 3dB lower than the peak. Thus we consider the equation

$$\sqrt{2}\bar{a}(\sigma = \sigma_{\frac{1}{2}}, \phi = -\frac{\pi}{4}) = \bar{a}(\sigma = 0, \phi = -\frac{\pi}{4})$$
 (2.21)

We assume a phase value of $\phi=-\frac{\pi}{4}$ to express the effective quality factor under maximum gain. It also proves necessary in order to make the equation

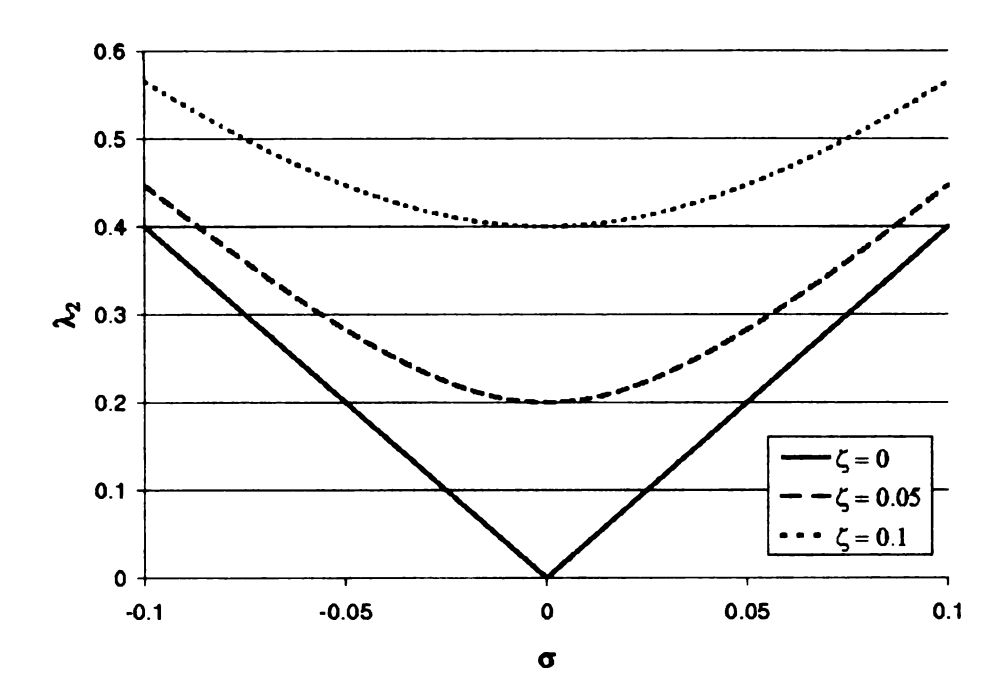


Figure 2.3. Wedge of instability near $\sigma = 0$. Note that parametric amplification requires that the operating point be below the wedge, as parametric resonance occurs above [1].

soluble. Accordingly, we find that

$$Q = \frac{1}{2\epsilon\sigma_{\frac{1}{2}}} \tag{2.22}$$

$$\sigma_{\frac{1}{2}} = \frac{1}{4} \sqrt{(4\zeta - \lambda_2)(-2\lambda_2 + \sqrt{4\lambda_2^2 + (\lambda_2 + 4\zeta)^2})}$$
 (2.23)

Here we find that the quality factor, Q, under no pump, $\lambda_2=0$, gives the classical result, $Q_0=\frac{1}{2\epsilon\zeta}$. We also find that under parametric excitation, the quality factor is monotonically increasing for pump values in the allowed range, $0\leq\lambda_2<\lambda_{2,crit}$.

2.1.3 Experimental Results

In this experiment, a spring steel beam, (190 mm × 19 mm × 0.5mm, $f_1 \approx 11.5 \; \mathrm{Hz}, \, f_2 \approx 73.3 \; \mathrm{Hz}$), was excited via base motion at an orientation of $\alpha=80^{\circ}$. The base motion was imposed by an MB Dynamics vibration exciter (model PM-500), and measured using a three-axis accelerometer (Analog Devices ADXL105EM-3) mounted directly on the exciter table. The beam response was measured using two strain gauges (Measurements Group Inc. Micro Measurements Division, EA-13-129LZ-120) mounted in a half-bridge configuration. The damping ratio of the beam was determined to be between $\epsilon \zeta \approx 0.005$ and $\epsilon \zeta \approx 0.009$, using the log decrement method. For the theoretical plots, $\epsilon \zeta \approx 0.007$ was used. Figure 2.4 shows the measured magnitude frequency response of the beam for three different pump values along with the theoretical response. These curves have been normalized by $max\{\bar{a}|\lambda_2=0\}$, the maximum of the unpumped response amplitude, such that the unpumped system has unit amplitude at the natural frequency. The result is that the theoretical curves have been normalized by the theoretical critical pump value, and the measured data has been normalized by the measured critical pump value. Figure 2.5 (a) shows the beam with no pump ($\lambda_2=0$), and figure 2.5 (b) shows the beam with the pump on ($\lambda_2 \neq 0$). The gain at resonance due to parametric amplification is described by equation (2.19), and plotted in figure 2.6. Here, the gain is plotted against pump amplitude, assuming a phase of -45° which is associated with maximum gain. The measured pump amplitudes were obtained from the accelerometer data. The theoretical gain curve becomes unbounded as the pump amplitude approaches critical, but the real system is not truly linear. It is only linear for small displacements, and so, we expect some finite measured gain as the pump reaches critical. The magnitude of the gain depends on both the magnitude of the nonlinearity and also

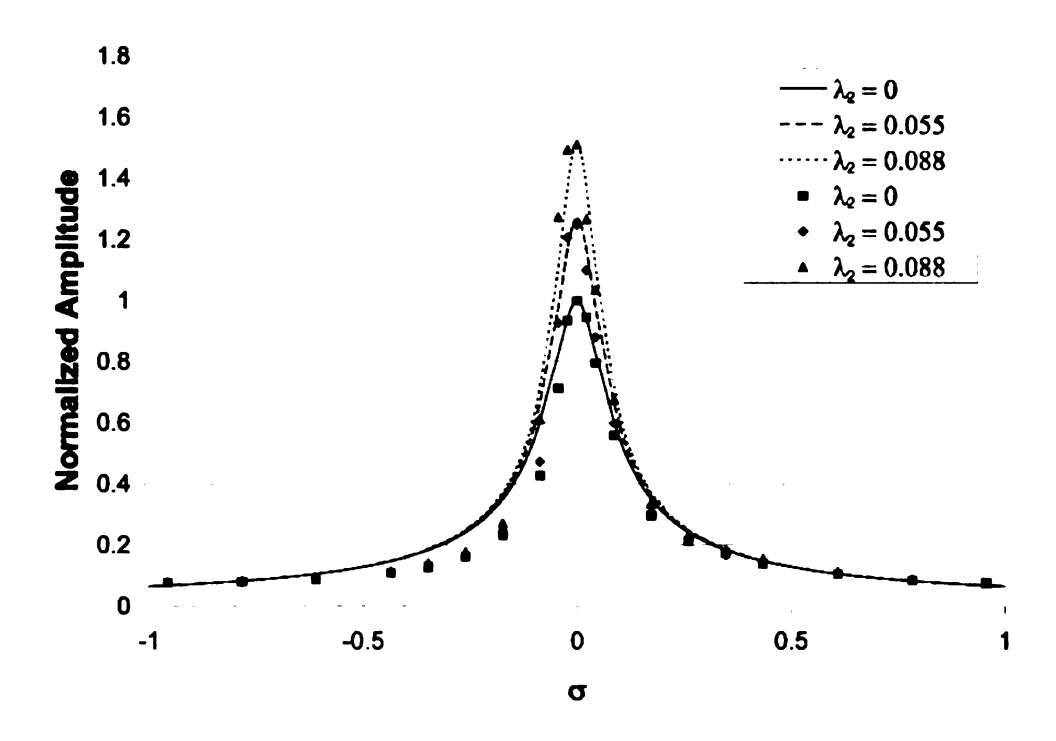
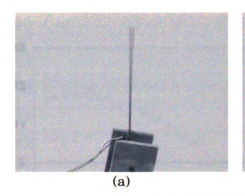


Figure 2.4. Frequency response for three parametric pump amplitudes [1]. The continuous lines indicate theoretical results, the points indicate measured data.

the magnitude of the forcing, since such amplitude dependence is characteristic of nonlinear systems. For the case here, we see that the beam reaches a gain of about 3. It should be possible to obtain larger gain by increasing the dynamic range of the parametrically amplified device, i.e., decreasing the nonlinear stiffness and noise floor. This investigation however, is beyond the scope of this work, and is left as a future endeavor.

The phase dependence of the gain in degenerate parametric amplification is illustrated in figure 2.7. Here, the response amplitude, normalized to 1 when the phase is zero, is plotted against the phase. Figure 2.7 shows the measured and theoretical phase dependence of the resonator amplitude. In line with the theoretical prediction, the measured data shows maxima and minima occurring near -45° and 45° respectively. This phase dependence is repeated on



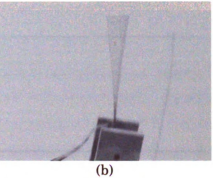


Figure 2.5. Time lapse photographs [1].

180° intervals

2.2 The Manley-Rowe Equations

In the illustration of degenerate parametric amplification above, power is delivered to a single resonator through parametric forcing. In a more general situation, where there are multiple parametrically coupled resonators, the power relationships are not so obvious. The Manley-Rowe equations, first detailed by Manley and Rowe in 1956 [34], can provide some insight, however. While these equations describe the average power relationships at different frequencies for nonlinear inductors and capacitors, by use of a small signal assumption, these equations can be used to analyze power transfer in multiple parametrically coupled resonators. Again, by parametrically coupled, we mean coupled with periodically time-varying coefficients. The derivation for these equations can be found in [34, 3, 5], and will not be repeated here. The Manley-Rowe equations assume that, given two nonzero incommensurate frequencies, ω_1 and ω_2 , the natural frequencies of all coupled resonators as well as the parametric variation frequency have nonzero values given by $m\omega_1 + n\omega_2$. Where m and n are integers, positive, negative, or zero. Then the average power at these frequencies frequency.

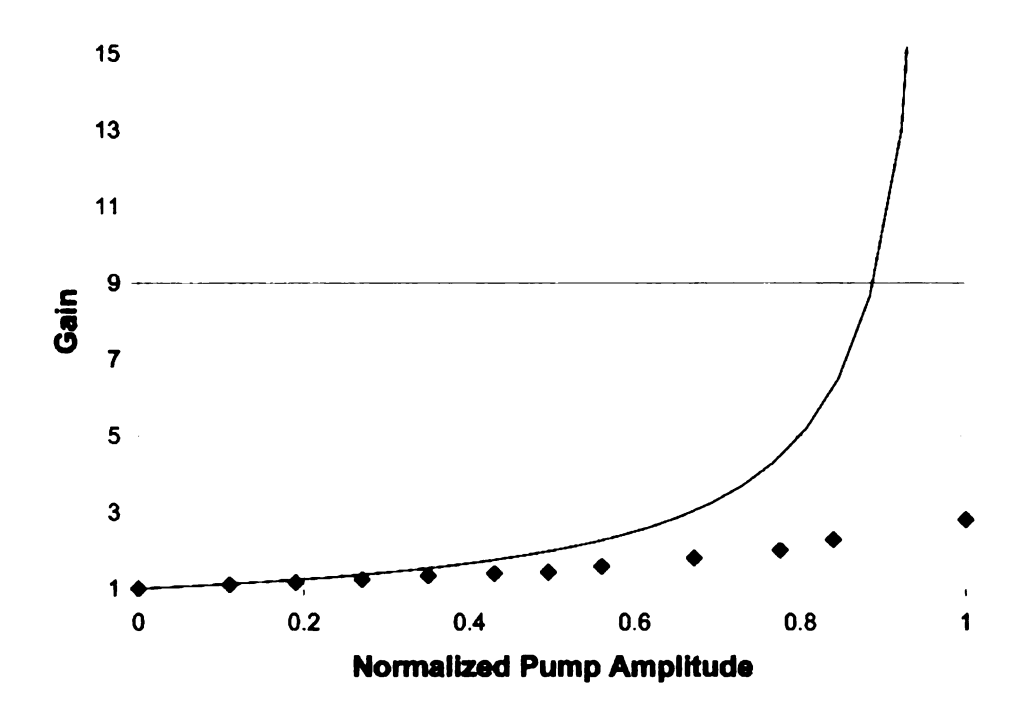


Figure 2.6. Gain vs normalized pump amplitude [1]. The pump amplitude is normalized such that $\lambda_{2,crit} = 1$. The continuous line indicates theoretical result, the points indicate measured data.

cies must obey the Manley-Rowe equations,

$$\sum_{m=0}^{\infty} \sum_{n=-\infty}^{+\infty} \frac{mP_{m,n}}{m\omega_1 + n\omega_2} = 0, \qquad (2.24)$$

$$\sum_{m=-\infty}^{+\infty} \sum_{n=0}^{\infty} \frac{nP_{m,n}}{m\omega_1 + n\omega_2} = 0.$$
 (2.25)

 $P_{m,n}$ is the average power at frequency $m\omega_1 + n\omega_2$, with the sign convention being that positive $P_{m,n}$ means power is absorbed by the nonlinear or time-varying parametric element, and power given out is negative. Or, alternatively, positive $P_{m,n}$ implies that power is drawn from frequency $m\omega_1 + n\omega_2$, and negative $P_{m,n}$ implies that power is given to frequency $m\omega_1 + n\omega_2$.

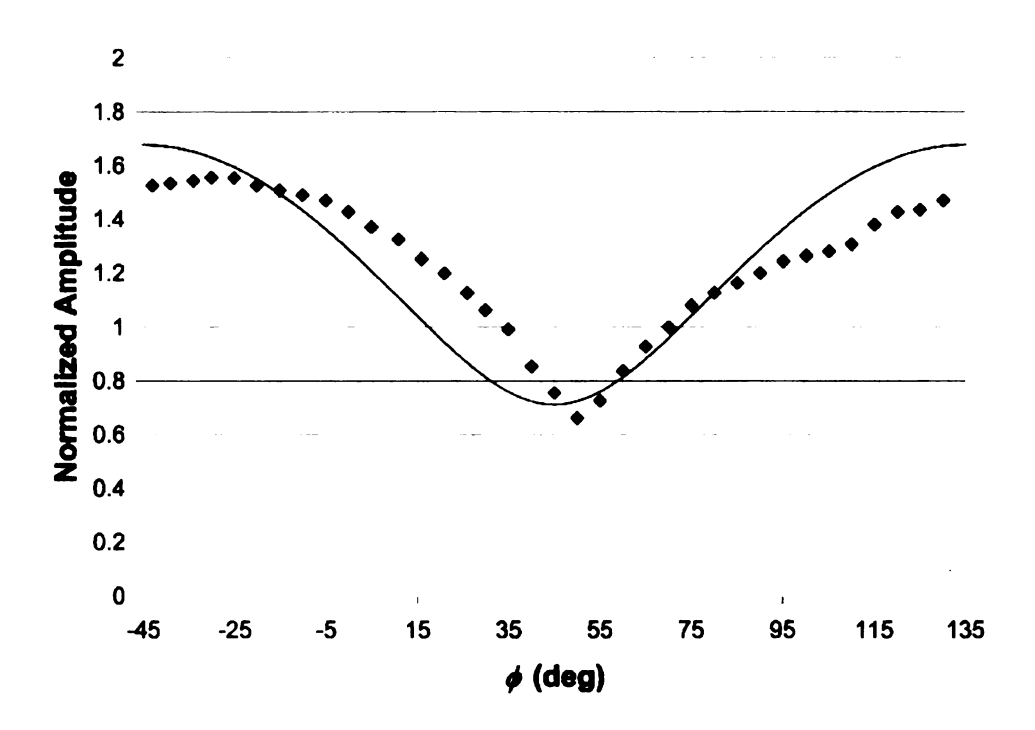


Figure 2.7. Gain vs phase [1]. The continuous line indicates theoretical results, the points indicate measured data.

2.3 Nondegenerate, Three-Frequency Amplifier

Though the Manley-Rowe equations describe power transfer for an arbitrary number of parametrically coupled resonators, let us now consider the simplest case where we have only two parametrically coupled resonators. Two parametrically coupled resonators can act as a three-frequency parametric amplifier operating in the non-degenerate mode (as mentioned in 1.1), and so here we present the three-frequency amplifier to explain, by illustration, non-degenerate parametric amplification. Non-degenerate amplification will be examined again in chapter 3, where we discuss a more general system of parametric resonators.

The three-frequency amplifier is made up of two parametrically coupled res-

onators, a signal resonator and an idler resonator. The signal resonator has fundamental frequency $\omega_s>0$, and is directly forced by the amplifier input signal. The idler resonator has fundamental frequency $\omega_i>0$, and is unforced. The three frequencies of the three-frequency amplifier are the fundamental frequency of each of the resonators and the frequency of variation of the coupling parameters, $\omega_p>0$. So, with regard to the Manley-Rowe equations we have signal power P_s at frequencies $\pm\omega_s$, idler power P_i at frequencies $\pm\omega_i$, and pump power P_p at frequencies $\pm\omega_p$. As there can only be two incommensurate frequencies we take

$$\omega_{i} = \begin{cases} \omega_{s} + r\omega_{p}, & \omega_{s} > -r\omega_{p} \\ -\omega_{s} - r\omega_{p}, & \omega_{s} < -r\omega_{p} \end{cases}$$
 (2.26)

where r is an integer. The Manley-Rowe equations, then, reduce to

$$\frac{P_s}{\omega_s} + \frac{P_i}{\omega_s + r\omega_p} = 0, (2.27)$$

$$\frac{P_p}{\omega_p} + \frac{rP_i}{\omega_s + r\omega_p} = 0. {(2.28)}$$

Some insight into the three-frequency amplifier can be obtained by rewriting equations (2.27) and (2.28) as

$$P_p = -rP_i \frac{\omega_p}{\omega_s + r\omega_p} = rP_s \frac{\omega_p}{\omega_s}$$
 (2.29)

When $\omega_s > -r\omega_p$, it is clear from (2.29) that P_s and P_i must have opposite signs. Thus the parametric excitation absorbs power from one resonator, and delivers power to the other. We can rewrite this frequency condition as $\omega_p = \frac{\omega_i - \omega_s}{r}$. The pump frequency, or frequency of parametric variation, ω_p , is commensurate with the difference of the resonator frequencies. Thus we say that the resonators are being pumped at a combination resonance of the difference type. In this situation, the device is said to be stable because, as we will

see, the parametric excitation cannot destabilize the resonators; it only affects the coupling between them.

When $\omega_s<-r\omega_p$, it must be that r<0, and that P_s and P_i both have the same sign. Thus both resonators gain energy if $P_p>0$ and lose energy if $P_p<0$. In this case the frequency condition can be rewritten as $\omega_p=\frac{\omega_i+\omega_s}{-r}$. The pump frequency is commensurate with the sum of the resonator frequencies. Thus we say that the resonators are being pumped at a combination resonance of the sum type. In this configuration the device is potentially unstable because the parametric excitation can destabilize the system. The three-frequency amplifier is usually constructed with r=-1 while maintaining the parametric excitation level beneath the instability threshold. Other values of r are theoretically possible, however, there are practical difficulties associated with those modes of operation [3], however.

Electrical examples of three-frequency amplifiers can be found in [3, 5]. Micro-mechanical examples can be found in [19, 8]. Generally, either type of system can be described with equations (2.30) and (2.31).

$$\ddot{x} + 2\epsilon \zeta_s \omega_s \dot{x} + \omega_s^2 (1 + \epsilon \delta \cos(\omega_p t)) x - \epsilon \gamma \delta \cos(\omega_p t) y = \epsilon A \cos(\omega_s t + \phi)$$
(2.30)

$$\ddot{y} + 2\epsilon \zeta_i \omega_i \dot{y} + \omega_i^2 (1 + \epsilon \delta \cos(\omega_p t)) y - \epsilon \gamma \delta \cos(\omega_p t) x = 0 \quad (2.31)$$

where x is the motion of the signal resonator, which has fundamental frequency ω_s , and y is the motion of the idler resonator, which has fundamental frequency ω_i . The signal to be amplified is applied as an input into the signal resonator at the resonators fundamental frequency, and the two resonators are parametrically coupled with coupling strength γ . The coupling term is sinusoidal with pump strength δ , and pump frequency ω_p which satisfies the relationship $\omega_i^2 = (\omega_p - \omega_s)^2 + \epsilon \sigma$. That is, the pump frequency is near $\omega_i + \omega_s$, the

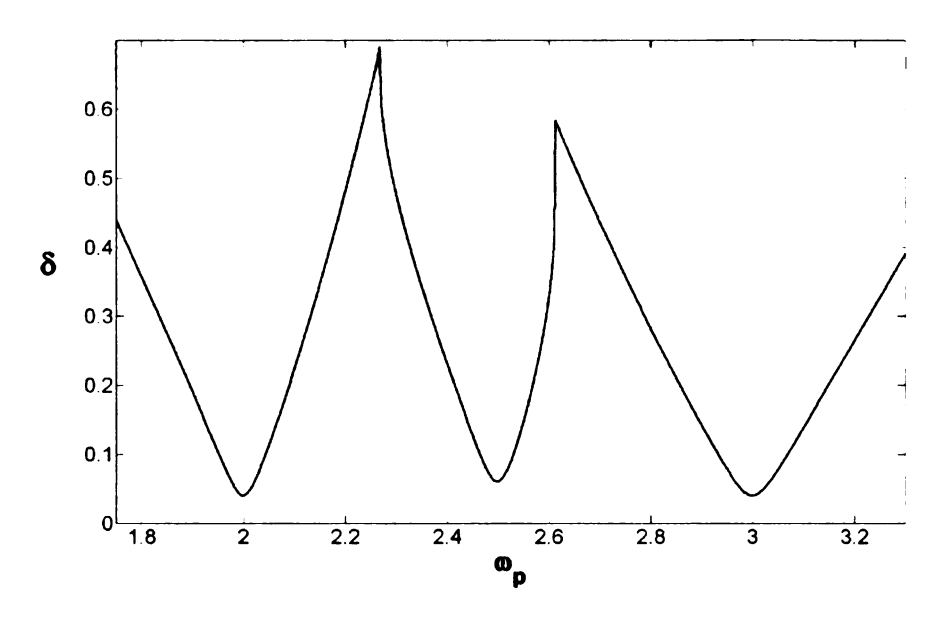


Figure 2.8. Wedges of instability for the non-degenerate resonator, for $\omega_s = 1$, $\omega_i = 1.5$, $\zeta_s = 0.01$, $\zeta_i = 0.01$, $\gamma = 1$, $\epsilon = 1$

first combination resonance of the sum type. If we examine the stability of the system in the ω_p , δ plane, we find that there are wedges of instability at $2\omega_i$, $2\omega_s$, and $\omega_i + \omega_s$. Figure 2.8 shows the ω_p , δ plane in the area of the wedges mentioned. Again, above the wedges is unstable, and below is stable. There are more wedges at lower values of ω_p , but the wedges shown, which are also the highest frequency wedges, are the most robust under increasing dissipation, and so are the ones usually used for parametric forcing. The wedge located at $2\omega_s$ is associated with the principle resonance of the signal resonator. Choosing a pump frequency under this wedge will degenerately amplify the signal resonator. Similarly, the wedge at $2\omega_i$ is associated with the principle resonance of the idler resonator. The wedge at $\omega_i + \omega_s$ is associated with the combination resonance, and choosing a pump frequency under this wedge will non-degenerately amplify both the signal and idler resonators.

So, by choosing the pump frequency as defined above and applying the

...

method of multiple scales to equations (2.30) and (2.31), we find that the equations have a solution of the form

$$x(t) = a(\epsilon t)\sin(\omega_s t) + b(\epsilon t)\cos(\omega_s t), \qquad (2.32)$$

$$y(t) = c(\epsilon t)\sin(\omega_i t) + d(\epsilon t)\cos(\omega_i t), \qquad (2.33)$$

where a, b, c, and d are governed by the slow flow equations

$$a' = -\zeta_s \omega_s a + \frac{\gamma \delta}{4\omega_s} d + \frac{A}{2\omega_s} \cos(\phi), \qquad (2.34)$$

$$b' = -\zeta_s \omega_s b + \frac{\gamma \delta}{4\omega_s} c + \frac{A}{2\omega_s} \sin(\phi), \qquad (2.35)$$

$$c' = \frac{\gamma \delta}{4\omega_i} b - \zeta_i \omega_i c - \frac{\sigma}{2\omega_i} d, \qquad (2.36)$$

$$d' = \frac{\gamma \delta}{4\omega_i} a + \frac{\sigma}{2\omega_i} c - \zeta_i \omega_i d. \tag{2.37}$$

For the case of zero mistuning, $\sigma=0$, this set of slow flow equations has a stable fixed point where

$$|x_0| = 8\sqrt{\frac{A^2\zeta_i^2\omega_i^4}{(16\zeta_s\omega_s\zeta_i\omega_i - (\gamma\delta)^2)^2}}$$
 (2.38)

$$|y_0| = 2\sqrt{\frac{A^2(\gamma\delta)^2}{(16\zeta_s\omega_s\zeta_i\omega_i - (\gamma\delta)^2)^2}}$$
 (2.39)

This fixed point is stable for

$$\delta < \frac{4\sqrt{\zeta_s \omega_s \zeta_i \omega_i}}{\gamma} \tag{2.40}$$

Equations (2.38) and (2.39) show that, as the pump magnitude approaches the critical value, the amplitudes of the signal and idler resonators approach infinity. The gain curve for the signal resonator is presented in figure 2.9. Again, gain is defined as amplitude with the pump divided by the amplitude without the pump, $G = \frac{|x_0|_{pumpoff}}{|x_0|_{pumpon}}$. Note that the expressions for $|x_0|$ and $|y_0|$ are independent of the phase between parametric and direct forcing. Also, we

	,	
26		

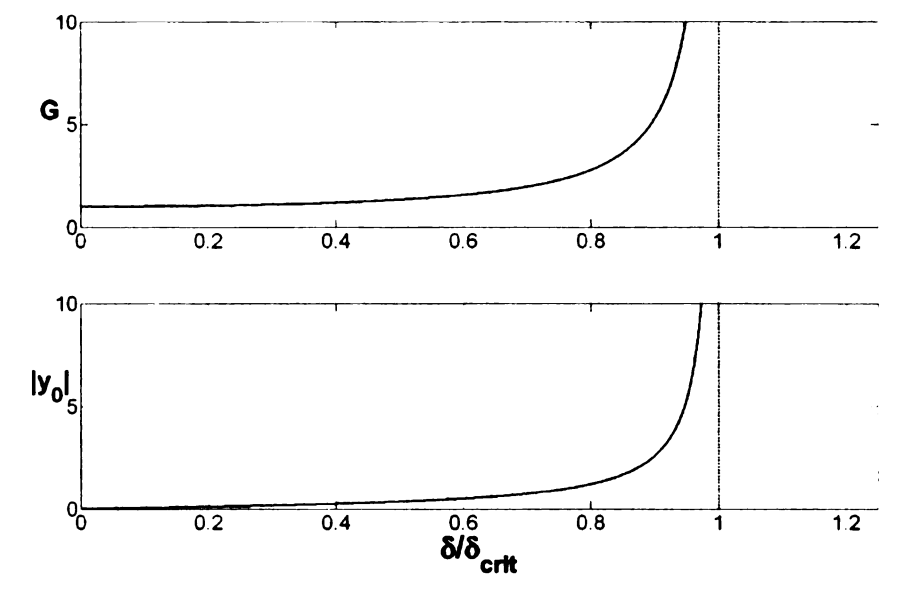


Figure 2.9. Gain of the non-degenerate resonator, for $\omega_s=1$, $\omega_i=1.5$, $\zeta_s=0.01$, $\zeta_i=0.01$, $\gamma=1$, $\epsilon=1$

see that sufficient pump amplitude will destabilize the system, as the Manley-Rowe equations suggest.

Let us momentarily consider parametrically forcing the system near a combination resonance of the difference type. This suggests the frequency condition $\omega_i^2 = (\omega_p + \omega_s)^2 + \epsilon \sigma$. The method of multiple scales again gives a solution in the form of equations (2.32) and (2.33), but with slow flow equations

$$a' = -\zeta_s \omega_s a + \frac{\gamma \delta}{4\omega_s} d + \frac{A}{2\omega_s} \cos(\phi), \qquad (2.41)$$

$$b' = -\zeta_s \omega_s b - \frac{\gamma \delta}{4\omega_s} c + \frac{A}{2\omega_s} \sin(\phi), \qquad (2.42)$$

$$c' = \frac{\gamma \delta}{4\omega_i} b - \zeta_i \omega_i c - \frac{\sigma}{2\omega_i} d, \qquad (2.43)$$

$$d' = -\frac{\gamma \delta}{4\omega_i} a + \frac{\sigma}{2\omega_i} c - \zeta_i \omega_i d. \tag{2.44}$$

These equations have a fixed point where, for zero mistuning ($\sigma = 0$),

$$|x_{0}| = 8\sqrt{\frac{A^{2}\zeta_{i}^{2}\omega_{i}^{4}}{(16\zeta_{s}\omega_{s}\zeta_{i}\omega_{i} + (\gamma\delta)^{2})^{2}}},$$

$$|y_{0}| = 2\sqrt{\frac{A^{2}\gamma^{2}\delta^{2}}{(16\zeta_{s}\omega_{s}\zeta_{i}\omega_{i} + (\gamma\delta)^{2})^{2}}}.$$
(2.45)

$$|y_0| = 2\sqrt{\frac{A^2\gamma^2\delta^2}{(16\zeta_s\omega_s\zeta_i\omega_i + (\gamma\delta)^2)^2}}.$$
 (2.46)

This fixed point is stable for all values of δ , thus confirming the claim we made in section 2.2 while discussing the Manley-Rowe result for the combination resonance of the difference type. Additionally, we see pumping the system decreases the amplitude of the signal resonator and increases the amplitude of the idler. Thus we see confirmation of the Manley-Rowe result which states that, for positive pump power, the time-varying stiffness element will take power from the signal resonator and provide power to the idler.

CHAPTER 3

Parametric Amplification in

Multi-Degree-of-Freedom Systems

In this chapter we analyze parametric amplification of multi-degree-of-freedom systems with distinct modal frequencies. We also assume that the parametric excitation has uniform and periodic time dependence. That is, the time varying stiffnesses of the system can be written as $K\underline{x}\Delta(t)$, where K is a constant matrix, \underline{x} is the vector of system coordinates, and $\Delta(t)$ is a periodic scalar function. This analysis is presented in section 3.1. In section 3.2, an example system is presented, in which parametric amplification is demonstrated. Numerical analysis of this is presented in section 3.2.1.

3.1 Analysis

Assuming small damping and forcing, and assuming small arbitrary parametric excitation, an N degree of freedom system can be described by

$$M\underline{x}'' + \epsilon C\underline{x}' + K_1\underline{x} + \epsilon K_2(\tau)\underline{x} = \epsilon F(\tau), \tag{3.1}$$

Where \underline{x} is an $N \times 1$ vector and M, C, K_1 , and $K_2(\tau)$ are the $N \times N$ mass, damping, constant stiffness, and variable stiffness matrices, respectively. $F(\tau)$ is the $N \times 1$ forcing vector. Though the system is linear, the solution cannot



be expressed as a tractable form of the transition matrix, and so, an approximation method is required. In this work we employ the method of multiple scales, after Nayfeh and Mook [33]. This method lends itself to identification and treatment of the various frequency conditions that arise. The complete first order multiple scales analysis is contained in appendix A, where the system is considered under five different frequency conditions. These five conditions correspond to the cases where the parametric excitation frequency is near an isolated primary resonance, an isolated combination resonance of the sum type, an isolated combination resonance of the difference type, simultaneous near both a combination resonance of the sum type and a combination resonance of the difference type, and, finally, near two combination resonances of the difference type. When we say that the parametric excitation frequency is near a resonance, we mean to imply that the frequency is near the tip of an instability wedge corresponding to that resonator. In the case of a multiple degree of freedom system, these resonators are simply the modes of the system. As we will see, the first case is analogous to the simple degenerate parametric amplifier discussed in section 2.1, and the second case is analogous to the three-frequency amplifier discussed in section 2.3.

In the presentation of this analysis, some of the steps have been left to the appendix since such steps are comprised of simple algebraic manipulation which add little to the discussion. So, to begin, let us clarify what is meant by the modes of the system. More precisely, we are referring to the modes of the unperturbed system, $M\underline{x}'' + K_1\underline{x} = 0$, which are represented by the coordinates $\underline{y} = U^T\underline{x}$. U is the similarity transform that decouples $M\underline{x}'' + K_1\underline{x} = 0$, and is normalized such that $U^TMU = I$. Thus we express the

equation of motion, (3.1) as

$$y_r'' + \omega_r^2 y_r = \epsilon \sum_{j=1}^N \left[-Z_{rj} y_j' - \Delta_{rj} y_j + U_{jr} F_j \right] \quad r = 1...N, \quad (3.2)$$

where $Z = U^T C U$ and $\Delta = U^T K_2 U$. Here y_r is the amplitude and ω_r is the frequency of the r^{th} mode. Note that the parametric forcing, $\Delta_{rj} y_j$, carries modal contribution factors since Δ is the transformation of K_2 by U.

Let us consider an isolated primary resonance, the first of the five cases listed above, and let this resonance be associated with the k^{th} mode. Also, let $\Delta_{rj} = \gamma_{rj}\cos(\Omega t + \phi) + \delta_{rj}\cos(2\Omega t)$ and $F_j = A_j\cos(\Omega t + \phi) + B_j\cos(2\Omega t)$, where $\Omega^2 = \omega_k^2 + \epsilon \sigma$. While only the 2Ω component of Δ_{rj} and the Ω component of F_j are required for parametric amplification, we have included the other terms because the parametric and direct forcings will share the same frequency content when they are both provided by the same mechanism. For example, electrostatic forcing provides direct and parametric forcing which are both proportional to the applied voltage squared.

The O(1) solution of the multiple scales equations gives

$$y_{k0} = X_1(\epsilon t)\cos(\Omega t) + Y_k(\epsilon t)\sin(\Omega t),$$
 (3.3)

where y_{k0} is the O(1) solution of y_k . The slowly time varying amplitudes, X_k , Y_k , of the sinusoids are governed by

$$X'_{k} = -\frac{1}{2}Z_{kk}X_{k} + \frac{\delta_{kk} + 2\sigma}{4\Omega}Y_{k} + \frac{F_{A}}{2\Omega}\sin(\phi),$$
 (3.4)

$$Y_k' = \frac{\delta_{kk} - 2\sigma}{4\Omega} X_k - \frac{1}{2} Z_{kk} Y_k - \frac{F_A}{2\Omega} \cos(\phi), \qquad (3.5)$$

where $F_A = \sum_{j=1}^N U_{jk} A_j$ is the effective force acting on the k^{th} mode. To arrive at these equations it is necessary to assert the frequency conditions

$$\omega_{i} \neq \omega_{j}, \quad i \neq j$$

$$\omega_{i} \pm \Omega_{j} \neq \omega_{k}, \quad i = 1...N \neq k$$
(3.6)

Here Ω_j represents all frequencies present in the parametric forcing, Δ_{kj} . These frequency conditions are required to isolate the k^{th} mode from all others. To see this result, consider equation (3.2). The $-Z_{kj}y_j'$ term will couple modes (to first order) only if those modes have the same frequencies. Thus we assert that no two modal frequencies are the same. The $-\Delta_{kj}y_j$ term will modulate the modal frequencies by the pump frequency, and potentially couple modes. Since we are considering an isolated mode, we generate these frequency conditions so that the k^{th} mode will not be coupled to any other mode. The above system has one fixed point, where

$$|y_{k0}| = 2 \left[\left(F_A^2 (\delta_{kk}^2 + 4\Omega^2 Z_{kk}^2 - 4\Omega Z_{kk} \delta_{kk} \sin(2\phi) + 4\sigma^2 + 4\sigma \delta_{kk} \cos(2\phi) \right) / (\delta_{kk}^2 - 4(\sigma^2 + \Omega^2 Z_{kk}^2))^2 \right]^{\frac{1}{2}}, \quad (3.7)$$

$$\angle y_{k0} = \tan^{-1} \left(\frac{(\delta_{kk} - 2\sigma) \sin(\phi) - 2\Omega Z_{kk} \cos(\phi)}{(\delta_{kk} + 2\sigma) \cos(\phi) - 2\Omega Z_{kk} \sin(\phi)} \right). \quad (3.8)$$

This fixed point is stable for

$$|\delta_{kk}| < 2\sqrt{\sigma^2 + \Omega^2 Z_{kk}^2}. (3.9)$$

When this fixed point is stable, it represents the steady state solution of y_k to first order. We can then compare this steady state solution to the case where no parametric excitation is applied. We describe this as the gain resulting from parametric amplification, G (the ratio of $|y_{k0}|$ with the pump and $|y_{k0}|$ without the pump), which can be expressed as

$$G(\sigma = 0) = 2\Omega Z_{kk} \sqrt{\frac{\delta_{kk}^2 + 4\Omega^2 Z_{kk}^2 - 4\Omega Z_{kk} \delta_{kk} \sin(2\phi)}{(\delta_{kk}^2 - 4\Omega^2 Z_{kk}^2)^2}}$$
(3.10)

for zero detuning, ($\sigma=0$). Figure 3.1 shows normalized gain curves for a range of phase values, ϕ , ranging from $\frac{-\pi}{4}$ to $\frac{\pi}{4}$. This range represents the entire spectrum of phase values since the phase dependence is cyclical. the

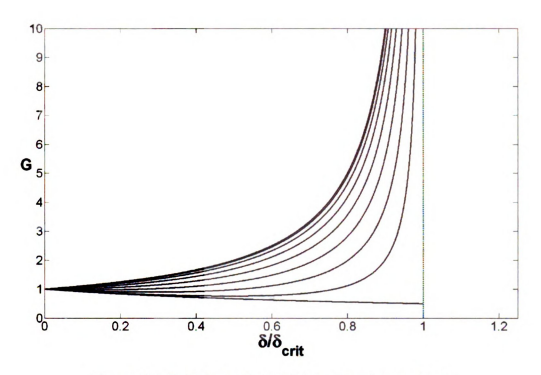


Figure 3.1. Gain curves for multiple scales solution, case 1.

maximum gain occurs at $-\frac{\pi}{4}$, and the minimum gain occurs at $\frac{\pi}{4}$. Inspection of these results show that this frequency condition produces behavior identical to the degenerate amplification example in section 2.1. Here we are degenerately amplifying a single mode of the system, while all other modes are unaffected by this mode's response. The other modes, however, may be coupled among themselves due to the parametric excitation.

For the second case, when the excitation frequency is near an isolated combination resonance of the sum type $(\omega_q + \omega_p)$, we take $\Delta_{rj} = \delta_{rj} \cos(2\Omega t)$ and $F_j = A_j \cos(\omega_q t + \theta) + B_j \cos(\omega_p t + \psi) + C_j \cos(\Omega t + \phi)$, where $2\Omega = \omega_p + \sqrt{\omega_q^2 + \epsilon \sigma}$ and $\omega_q^2 = (2\Omega - \omega_p)^2 - \epsilon \sigma$. In this case, we are only using the necessary frequency in the parametric term, Δ_{rj} , with the understanding that any other frequencies included here will complicate the frequency conditions, but not change the result. Thus we assert that the parameter of the parameter of the complex conditions are considered as $\Delta_{rj} = \Delta_{rj} \cos(2\Omega t)$.

metric excitation frequency is near the sum of the frequencies for modes p and q. Also, we have added direct forcing at the corresponding modal frequencies.

Considering the modes p and q, we again find that the O(1) equations give sinusoids with slow amplitude variation.

$$y_{p0} = X_p(\epsilon t)\cos(\omega_p t) + Y_p(\epsilon t)\sin(\omega_p t)$$
 (3.11)

$$y_{q0} = X_q(\epsilon t)\cos((2\Omega - \omega_p)t) + Y_q(\epsilon t)\sin((2\Omega - \omega_p)t)$$
 (3.12)

where y_{p0} and y_{q0} denote the O(1) solutions of modes p and q. The slowly time varying amplitudes are governed by the differential equations

$$X_p' = \frac{\delta_{pq}}{4\omega_p}Y_q - \frac{1}{2}Z_{pp}X_p + \frac{F_B}{2\omega_p}\sin(\psi)$$
 (3.13)

$$Y_p' = \frac{\delta_{pq}}{4\omega_p} X_q - \frac{1}{2} Z_{pp} Y_p - \frac{F_B}{2\omega_p} \cos(\psi)$$
 (3.14)

$$X_q' = -\frac{1}{2}Z_{qq}X_q - \frac{\sigma}{2\omega_q}Y_q + \frac{\delta_{qp}}{4\omega_q}Y_p + \frac{F_A}{2\omega_q}\sin(\theta)$$
 (3.15)

$$Y_q' = -\frac{\sigma}{2\omega_q} X_q - \frac{1}{2} Z_{qq} Y_q + \frac{\delta_{qp}}{4\omega_q} X_p - \frac{F_A}{2\omega_q} \cos(\theta)$$
 (3.16)

where $F_A = \sum_{j=1}^N U_{jq} A_j$ and $F_B = \sum_{j=1}^N U_{jp} B_j$ are the effective forcing values for modes p and q. To arrive at these equations it is necessary to assert that, again, no two modes have the same frequency, and

$$|\omega_i \pm \Omega_i| \neq |\omega_p| \qquad i \neq q,\tag{3.17}$$

$$|\omega_i \pm \Omega_i| \neq |\omega_a| \qquad i \neq p. \tag{3.18}$$

Again, here, Ω_j represents all frequencies present in the parametric force. These conditions state that no mode will couple to the p^{th} or q^{th} mode by modulation of its frequency by any frequency in the parametric force. Note that this condition does not contradict the conditions for the first case as long as $k \neq p, q$. So, we can have parametric excitation near both the combination

resonance and a principle resonance, and the two will not interact. Furthermore, if we are near multiple combination resonances, they will not interact as long as each combination resonance belongs to a distinct pair of resonators. The slow flow equations for this case have a fixed point with modal amplitudes

$$|y_{p0}| = 2 \left[\left(F_A^2 \delta_{pq}^2 + 4 F_B^2 (\sigma^2 + Z_{qq}^2 \omega_q^2) + 4 F_A F_B \delta_{pq} (\sigma \cos(\theta + \psi) - Z_{qq} \omega_q \sin(\theta + \psi)) \right) / (16 \sigma^2 Z_{pp}^2 \omega_p^2 + (\delta_{pq} \delta_{qp} - 4 Z_{pp} Z_{qq} \omega_p \omega_q)^2) \right]^{\frac{1}{2}}$$
(3.19)

and

$$|y_{q0}| = 2\sqrt{\frac{F_B^2 \delta_{qp}^2 + 4F_A^2 Z_{pp}^2 \omega_p^2 - 4F_A F_B Z_{pp} \delta_{qp} \omega_p \sin(\theta + \psi)}{16\sigma^2 Z_{pp}^2 \omega_p^2 + (\delta_{pq} \delta_{qp} - 4Z_{pp} Z_{qq} \omega_p \omega_q)^2}}. \quad (3.20)$$

This fixed point is stable for

$$\delta_{pq}\delta_{qp} < \frac{4\omega_p Z_{pp} Z_{qq} (\sigma^2 + \omega_q^2 (Z_{pp} + Z_{qq})^2)}{\omega_q (Z_{pp} + Z_{qq})^2}.$$
 (3.21)

Thus, parametric excitation near a combination resonance of the sum type can only be made unstable if the signs of δ_{pq} and δ_{qp} are the same. This will be the case for a symmetric parametric excitation matrix, K_2 in equation (3.1). This frequency condition produces behavior similar to the non-degenerate example in chapter 2, except here both resonators (modes) are forced. Three-frequency amplification is possible if one of these two modes remains unforced to act as the idler resonator.

In the third case, where the excitation frequency is near an isolated combination resonance of the difference type $(\omega_q - \omega_p)$, we take the same excitation form as in the second case. Here we find that the result is the same as in the second case except for the substitutions $\omega_p \to -\omega_p$ and $\psi \to -\psi$. Thus we

have a steady state with amplitudes

$$|y_{p0}| = 2 \left[\left(F_A^2 \delta_{pq}^2 + 4 F_B^2 (\sigma^2 + Z_{qq}^2 \omega_q^2) + 4 F_A F_B \delta_{pq} (\sigma \cos(\theta - \psi) - Z_{qq} \omega_q \sin(\theta - \psi)) \right) / (16 \sigma^2 Z_{pp}^2 \omega_p^2 + (\delta_{pq} \delta_{qp} + 4 Z_{pp} Z_{qq} \omega_p \omega_q)^2) \right]^{\frac{1}{2}}$$
(3.22)

and

$$|y_{q0}| = 2\sqrt{\frac{F_B^2 \delta_{qp}^2 + 4F_A^2 Z_{pp}^2 \omega_p^2 + 4F_A F_B Z_{pp} \delta_{qp} \omega_p \sin(\theta - \psi)}{16\sigma^2 Z_{pp}^2 \omega_p^2 + (\delta_{pq} \delta_{qp} + 4Z_{pp} Z_{qq} \omega_p \omega_q)^2}}, \quad (3.23)$$

which are stable for

$$\delta_{pq}\delta_{qp} > -\frac{4\omega_{p}Z_{pp}Z_{qq}(\sigma^{2} + \omega_{q}^{2}(Z_{pp} + Z_{qq})^{2})}{\omega_{q}(Z_{pp} + Z_{qq})^{2}}.$$
 (3.24)

We see that combination resonances of the difference type can only be made unstable if the signs of δ_{pq} and δ_{qp} are different. Consequently, when K_2 , the parametric excitation matrix, is symmetric, we cannot destabilize a combination resonance of the difference type. We can, however, move vibration energy from one mode to another while pumping near a combination resonance of the difference type. To see this, consider the case where we have $F_A \neq 0$, $F_B \neq 0$, and $\sin(\theta - \psi) = -1$. A choice of $\delta_{pq} = \delta_{qp} = 2\frac{F_A}{F_B}Z_{pp}\omega_p$ will drive $|y_{q0}| \to 0$, and $|y_{p0}|$ will go to some finite value. In addition, note that this choice of parametric excitation remains in the stable region. Note that to do this we require that the mode to which the energy is transfered be forced, and that this forcing have a specific phase relative to the forcing of the mode whose amplitude is to be suppressed.

The fourth and fifth cases are more complicated. Here the parametric excitation is near a combination resonance belonging to three resonators. The analysis for these cases provide slow flow equations, but we have not been able to produce analytic stability conditions or other results from these equations.

3.2 Parametrically Amplified Frequency Sweeping: An Application Illustrated by Example

We now consider an example application of the above results. DeMartini et al. have presented a novel sensing strategy for a resonant chemical-mass sensor [2]. This sensing scheme employs vibration localization in a multi-degree-of-freedom mechanical microresonator to allow identification of resonant frequency shifts in an array of chemical sensors. Yet, while this device gathers information from an entire array of chemical sensors, it employs only a single input and a single output. An experimental proof of concept is presented by DeMartini et al. [2]. An S.E.M. image of the device is shown in figure 3.2.

In these types of mass sensors, i.e., those that identify the presence of the target analyte by induced shifts in resonant frequency, damping in the resonators is an important issue. The minimum detectable mass of such devices is inversely related to the square root of the quality factor of the resonator [35]. The dominant source of damping in cantilever beam type resonators operating in air or liquid is dissipation associated with the surrounding fluid [36, 37]. As a result, it is not uncommon to see proof of concept testing in partial vacuum. Those who have reported extremely high sensitivity, such as Yang et al. [38] for example, exclusively (to the author's knowledge) operate in partial vacuum. DeMartini et al. were forced to do their proof of concept testing in vacuum as well "since the resonances were not sufficiently prominent at 1 atm, due to the small Q values associated with the resonance peaks of interest." [2].

This, of course, is somewhat problematic because the vacuum prevents the device from interacting with its environment, which is necessary to sense for the presence of the target analyte. Various methods have been employed in order to circumvent this problem. Burg et al. designed a resonant mass sen-

sor that operates in an external vacuum while channeling fluid from the environment in micro channels on the inside of the resonator [39]. The inside of the resonator is functionalized, so that the target analyte sticks to it, changing its resonant frequency by altering its mass and stiffness. Because the resonator operates in external vacuum, the damping caused by fluid drag is largely averted. Tamayo $et\ al$. applied derivative feedback to cantilever mass sensors in order to combat fluid damping [40]. This technique was applied to a cantilever in both air $(Q\ of\ 100)$, and liquid $(Q\ of\ 1)$. The effective $Q\ of\ the$ cantilever in liquid was increased to about 625. Mertz $et\ al$. also applied control to a microcantilever to regulate its response [41]. Dufour $et\ al$. showed that operating a cantilever in the strong-axis bending mode rather than the weak-axis bending mode reduces the effecting damping significantly [42]. Gallacher $et\ al$. [27] achieved $Q\ enhancement$ with parametric amplification.

Although some, or even all, of these methods could potentially be applied to the single input single output sensor, and indeed many are being investigated, here we explore only parametric amplification in an effort to, like Gallacher et al., improve the quality of a resonant sensor. This seems appropriate since this sensor has both the required frequency separation and the need for high quality resonances. We begin with a description of the device presented by DeMartini et al., which amounts to a summary of [2]. As such, many of the figures have been borrowed with permission from [2].

This single input single output sensor consists of several small resonators (cantilevered microbeams) coupled to a collective base, or shuttle mass, through which both forcing and sensing are applied. The device is designed in such a way that each of the sensing resonators exhibits localized behavior as a result of frequency separation of the system's various modes. This localized behavior is observed through the response of the shuttle mass, and so it is pos-

sible to observe frequency shifts in the sensing resonators by monitoring only the response of the shuttle mass.

Figure 3.2 shows a scanning electron micrograph of the device built for proof of concept. The shuttle mass, labeled SM, is attached to ground by four folded beam supports, labeled S, and forced by banks of interdigitated comb drives, labeled CD. The shuttle mass is connected to four microbeams, labeled M. The microbeams each have different lengths to allow for frequency separation. A lumped mass model used for the following analysis is shown in figure 3.3. The shuttle mass is represented by M, and the microbeams by m_i . The equations of motion are easily determined to be

$$M\ddot{x} + \sum_{i} m_{i} (\ddot{x} + \ddot{z}_{i}) + \sum_{i} c_{bi} (\dot{x} + \dot{z}_{i}) + c_{b}\dot{x} + k_{b}x = f(t),$$
 (3.25)

$$m_i(\ddot{x} + \ddot{z}_i) + c_{hi}(\dot{x} + \dot{z}_i) + c_i\dot{z}_i + k_iz_i = 0, \qquad i = 1, \dots, N$$
 (3.26)

where z_i is the relative displacement of the ith subsystem, given by

$$z_i = y_i - x, \qquad i = 1, \dots, N.$$
 (3.27)

Nondimensionalizing equations (3.25) and (3.26), and shifting the zero value of x, the equations of motion for this system can be written in the standard way.

$$M\underline{x''} + C\underline{x'} + K\underline{x} = F(\tau), \tag{3.28}$$

where M is the effective mass matrix, C the damping matrix, K the stiffness matrix, \underline{x} the compiled state vector, and $F(\tau)$ the forcing vector. For the single input, single output sensor, only the first element of the forcing vector is nonzero.

Figure 3.4 shows the desired frequency response for the system. That is, the qualitative frequency response which is in keeping with the necessary frequency separation and inertia ratio conditions which are required for this sensor scheme. Figure 3.4 (a) shows the frequency response magnitude for both

the shuttle mass and the microbeams and figure 3.4 (b) shows the phase for the shuttle mass only. In the shuttle mass magnitude response there are five resonance peaks, one for the bulk mode of the device, labeled 1, and one for each localized mode which corresponds to a single microbeam, labeled A-D. The corresponding experimentally obtained frequency response is shown in figure 3.5. Note that the experimental frequency response contains both the inplane modes predicted by theory, but also some out of plane modes, labeled 2 and 3, which were not captured by the model, but were predicted by finite element software.

In order to illustrate this device's function as a mass sensor, a 38pg platinum patch was deposited on the shortest microbeam, the one associated with resonance D. An SEM image of the platinum patch is shown in figure 3.6. Figure 3.7 shows experimentally obtained frequency responses in the neighborhood of the microbeam resonances, both with and without the platinum patch load. Because of the coupled nature of the device, all the resonance peaks move as a result of the platinum patch being applied to only one beam. Yet, the localized behavior of the modes ensures that the resonance associated with the microbeam carrying the load is shifted a great deal more than the others. Figure 3.8 shows the shift in resonance D as a result of the platinum patch. The shift is 124 Hz. Figure 3.9 shows the shift in the next resonance, resonance C, which shifts about 3 Hz. The shift in resonance D was about 40 times that of the other peaks.

3.2.1 Numeric Analysis

In order to illustrate parametric amplification in the single input single output sensor, and support the analysis above, we now consider a four microbeam numeric model, using equations (3.25) and (3.26), with parameters chosen similar

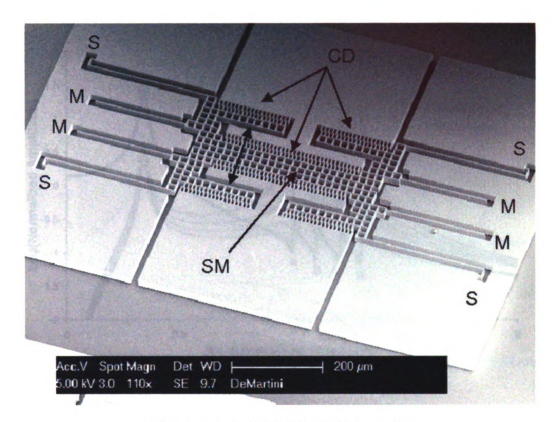


Figure 3.2. An SEM of the SISO device [2]

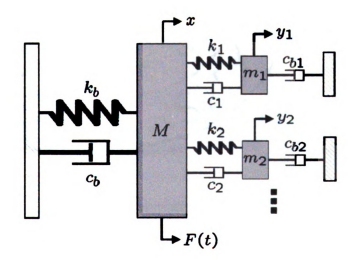


Figure 3.3. Lumped mass model of SISO device [2]

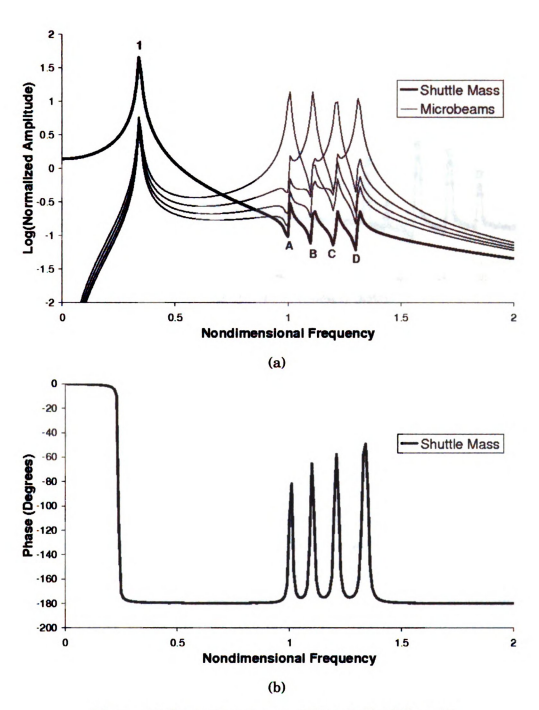


Figure 3.4. Frequency response. a) Magnitude, b) Phase [2].

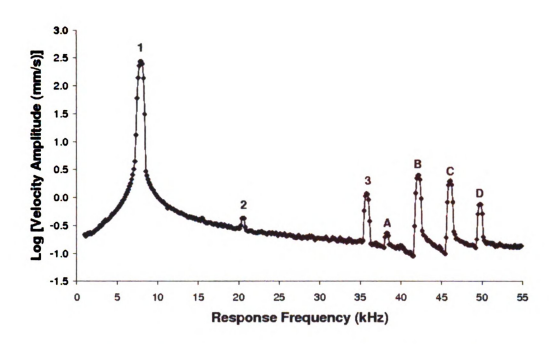


Figure 3.5. Experimental frequency response taken at $6.2\,\mathrm{V}$ AC in $275\mathrm{m}$ Torr pressure [2].

to the device presented by Demartini et al. [2]. We feel that this model captures the qualitative features of a general device, and so simulation results using this model provide a good qualitative understanding of the technique. The bode plot for the numerical model is shown in figure 3.10. Note that the frequency response contains the same features as those in figure 3.10, i.e., those amenable to mass sensing. A close up of the microbeam resonances is shown in figure 3.11. The resonant peaks shown in figure 3.11 correspond to those labeled A, B, C, and D in figure 3.4. In this model, these four resonances have achievable Q values of 97, 60, 65, and 56, respectively. The bulk mode has a Q value of 46.

For this example, we assume that the parametric excitation is applied at the device input, in the same way as the direct excitation. This could be accomplished via electrostatic forcing or feedback. We feel that this is in keep-

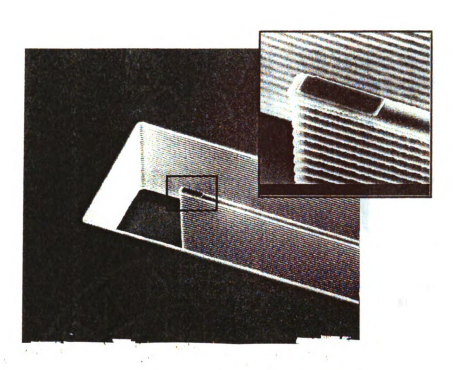


Figure 3.6. SEM image of platinum patch [2].

ing with the single input single output nature of this device, but also may be the simplest way to introduce parametric forcing to existing devices. Thus we take $(K_2)_{ii} = \delta \cos(2\Omega t)$ to be the only nonzero component of the parametric forcing matrix (see equation (3.1)). Here we denote the input coordinate to be x_i . Also the forcing vector F will have only one nonzero component, $F_i = A\cos(\Omega t + \phi)$. As such we expect degenerate parametric amplification on primary resonances, and the combination resonances will not generate responses because the modes associated with combination resonances will experience no direct forcing. Under this configuration, the stability regions in the Ω , δ plane are shown in figure 3.13, where the device is unstable above the curve, and stable below it. Again, recall that δ is the amplitude of the parametric forcing term. Here, in figure 3.13, the pump magnitude on the y-axis has been scaled such that a value of 1 corresponds to the pump value where the

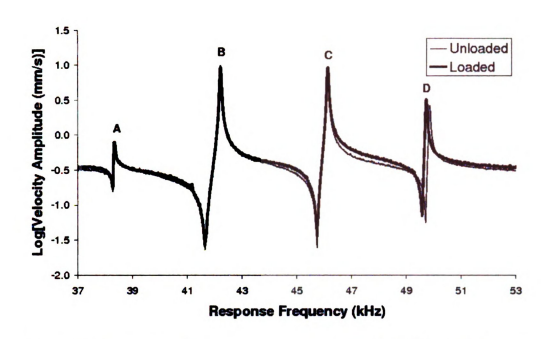


Figure 3.7. Experimental frequency response taken at 12.2~V~AC in 275mTorr pressure [2].

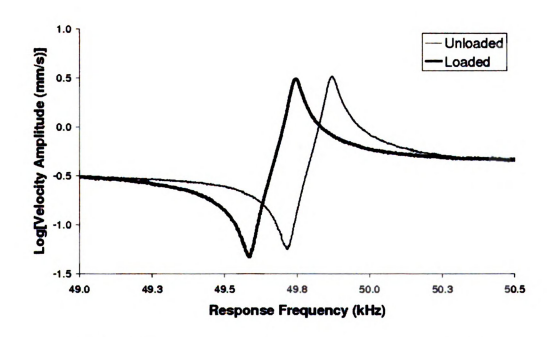


Figure 3.8. Experimental frequency response near resonance D [2].

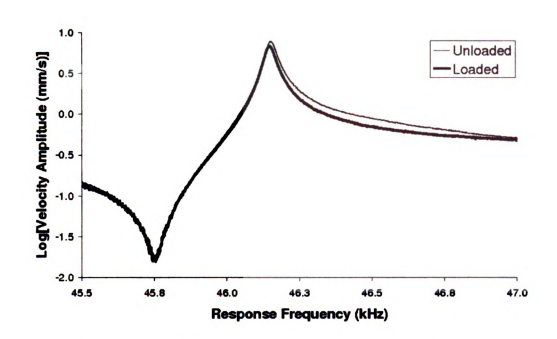


Figure 3.9. Experimental frequency response near resonance C [2].

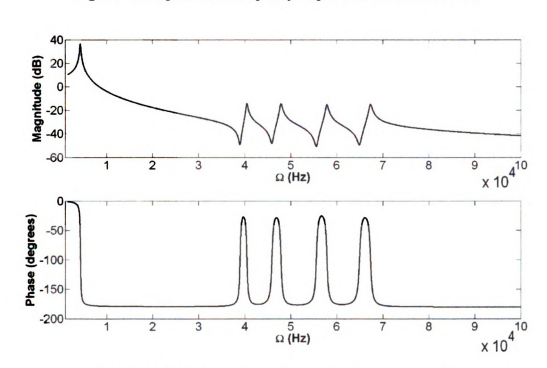


Figure 3.10. Bode plot for SISO model used for simulation

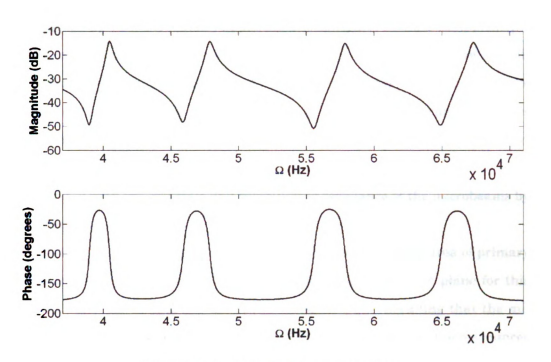


Figure 3.11. Close up of beam resonances

magnitude of the time varying stiffness matches that of the constant stiffness term. That is, the shuttle mass suspension stiffness, k_b (see figure 3.3) is no longer locally passive for all time when $\epsilon\delta U_{ii}^2/\omega_i^2>1$. This curve was produced using Floquet techniques. Note that because the factor of 2 is explicitly included in the parametric forcing term, principle resonance tongues appear at the fundamental frequencies of the modes, rather than at twice the fundamental frequency as in the discussion of parametric amplification in chapter 2. Also, the combination resonance tongues appear at the average of the frequencies of the two combinationally resonant modes, rather than the sum.

The Ω , δ plane shown in figure 3.12 has been divided up into three regions, where the wedges correspond with different behaviors. In region I, the primary instability wedge is located at the frequency of the primary bulk mode of the device. The additional wedges come from the infinite number of wedges

that stack up as the frequency approaches zero. Again, because each principle resonance produces a wedge at $\Omega = \frac{\omega}{n}$, for n=1,2,..., there are an infinite number in close proximity as $\Omega \to 0$. The wedges in region II are the result of the complicated interactions of the half frequency principle wedges of the microbeams (n=2), and the combination wedges generated by interactions of the frequencies in regions I and III. Region III contains ten wedges associated with the principle and combination resonance of the microbeams by themselves.

As the frequency range of the microbeam resonances is the area of primary interest, Figure 3.13 shows the stability boundary in the Ω , δ plane for this region. The ten wedges are labeled by number, 1-10. Recalling that the microbeam resonances were labeled A, B, C, and D, we can identify the resonances associated with each tongue. Tongue 1 is a principle resonance tongue for resonance A. Tongue 2 is a combination resonance between A and B. Tongue 3 is a principle resonance for B, and tongue 4 is a combination resonance for A and C. Tongue 5 is a combinations resonance for both B and C, and tongue 6 is a combination resonance for A and D. Tongue 7 is a combination resonance for B and D, and tongue 8 is a principle resonance for C. Tongue 9 is a combination resonance for C and D, and finally, tongue 10 is a principle resonance for D.

The dotted line in figure 3.13 shows the multiple scales prediction of the stability boundary. Note that, on the boundary, the pump value is significantly greater than the threshold of passivity $(\epsilon \delta U_{ii}^2/\omega_i^2=1)$. Thus, in the bulk mode equation, equation (3.2) with r=i, we have exceeded the $O(\epsilon)$ assumptions. However, in the higher mode equations, since $\omega_r>\omega_i$ $(r\neq i)$, we are merely approaching the limit of the $O(\epsilon)$ assumptions on the pump amplitude. For this reason, in figure 3.13, the multiple scales solution does capture the tongues fairly accurately, but does not capture the boundary feature labeled B,

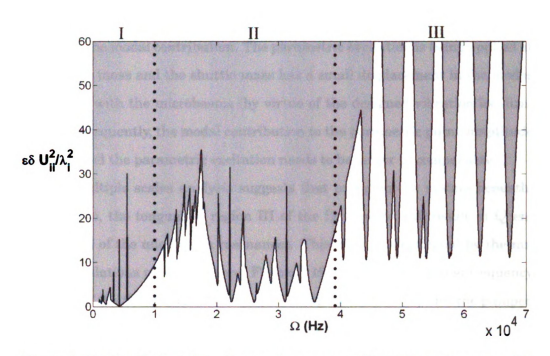


Figure 3.12. Stability boundary. Gray regions are unstable, white regions are stable

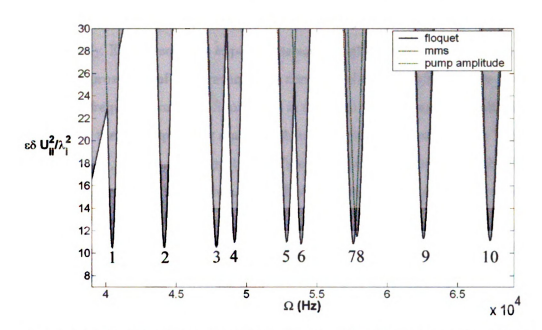


Figure 3.13. Stability boundary around beam frequencies. Gray regions are unstable, white regions are stable

which is associated with lower frequencies. The reason for the large pump amplitude is the modal contribution. The parametric excitation is being applied at the shuttle mass and the shuttle mass has a small displacement in the modes associated with the microbeams (by virtue of the designed vibration localization). Consequently, the modal contribution to the parametric pump amplitude is small, and the parametric excitation needs to be larger to compensate.

The multiple scales analysis suggests that pumping the system beneath, but close to, the tongues in region III of the Ω , δ plane will result in Q enhancement of the microbeam resonances. This effect is illustrated by the numeric simulations presented here. Figure 3.15 shows the simulated frequency response of the SISO model from quasi-static frequency sweeps for the pumped and unpumped cases along with the multiple scales prediction of the pumped case. The pump value, $\delta(\Omega)$, is shown in figure 3.14. Note that the pump value is below the stability boundary. The Q factors for resonances A, B, C, and D increased from 98.8, 89.4, 102.0, and 125.7 to 261.2, 220.6, 207.3, and 241.3 respectively. Each resonance experiences somewhat different levels of gain because the proximity of each resonance's corresponding instability wedge to the pump vs. frequency curve in figure 3.14 is different. The pumping amplitudes, relative to the corresponding stability threshold, for each resonance is 75.9%, 75.4%, 73.8%, and 71.9% respectively. Figure 3.16 shows a close up of the first resonance. From this figure we can see that the perturbation solution is indeed close to the real solution.

The parametrically amplified frequency sweeping technique we have illustrated here provides resonance quality enhancement without dependence on complete knowledge of the system parameters. We only require that the resonances we wish to amplify do not couple to other modes under degenerate parametric amplification and that we do not exceed the threshold of stability.

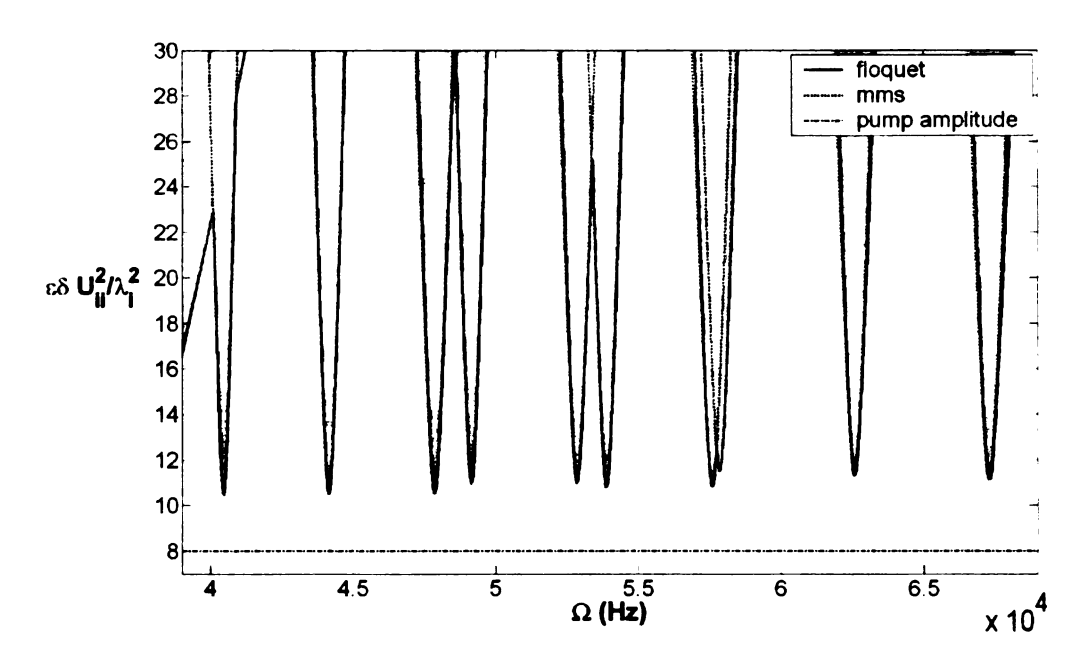


Figure 3.14. Pump value vs. frequency for multiple scales solution. Shown against stability boundary. Again, gray regions are unstable, and white regions are stable

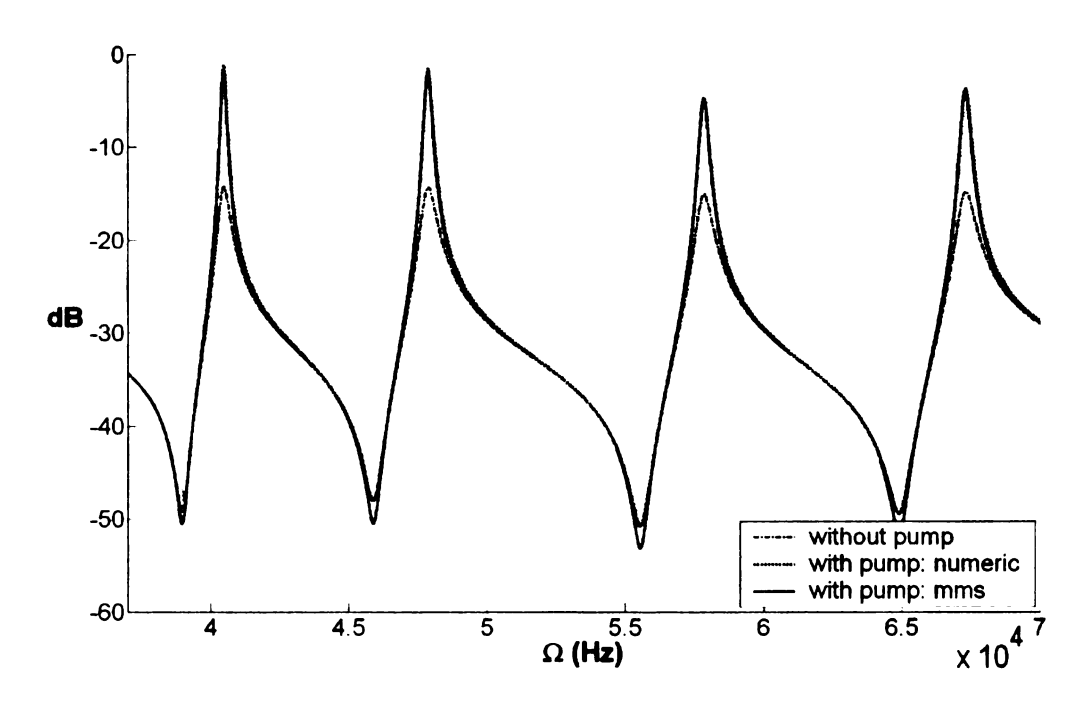


Figure 3.15. Numerical simulation of the pumped system

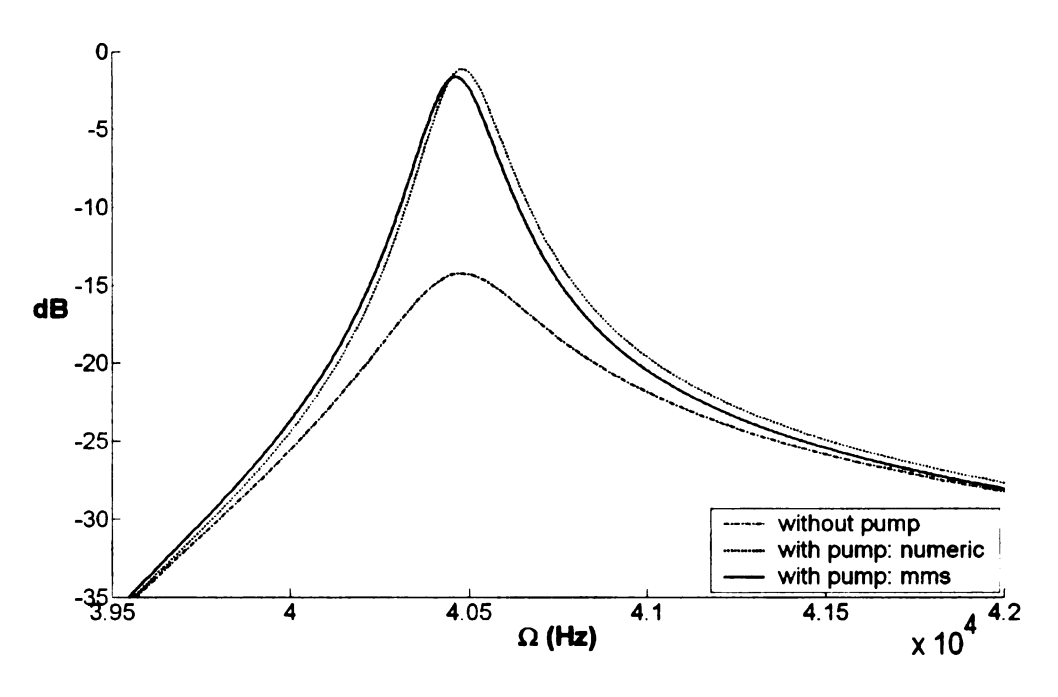


Figure 3.16. Close up of the first resonance for the numerical simulation of the pumped system

This sets the technique presented here apart from other approaches. Moving the poles by feedback control requires knowledge or estimation of those poles, and since our system functions by changes in resonant frequencies, these approaches may be more difficult to implement. Even vibrational control, as presented in [13, 14], requires that one know the system poles in order that they may be place properly by control. Still, this frequency sweeping method is closely related to vibrational control, and indeed could be thought of as placing poles by vibrational control. The difference, however, is that rather than placing all the poles with one parametric forcing signal, we are placing the poles one pair at a time as we come upon them, so to speak, in the frequency sweep.

CHAPTER 4

Conclusions and Future Work

In this thesis we discussed parametric amplification in multi-modal mechanical systems. Parametric amplification is an important issue in micro-electromechanical systems because such systems often require high resonance quality and are often forced in a manner where parametric effects are present. For example, it is often desirable to build devices on silicon-on-insulator wafers for ease of fabrication. It is also often convenient to force such devices electrostatically by applying a voltage between the device above the insulator, and the substrate below. Again, this is often done because it is simple and convenient. Such electrostatic forcing inherently produces parametric effects which can be taken advantage of. It is common, however, to think of parametric amplification in the form that it was presented by Rugar and Grütter [7], namely, degenerate amplification of a single resonator. We introduced degenerate parametric amplification in this way, showing, for the first time known to the author, parametric amplification in a macro-scale system. In this work we also show that parametric excitation has more versatility than this. Here we demonstrate that, for devices with proper frequency separation, one can use degenerate parametric amplification to piggy-back Q enhancement on a frequency sweep. This parametric effect can raise peak levels and quality factors of resonance peaks while leaving the nonresonant frequency response unchanged. Such a technique could be very useful for devices which rely on resonance location via frequency sweeping such as the single-input-single-output chemical-mass sensor we discussed in chapter 3. In addition, we showed that non-degenerate parametric amplification can be employed to either amplify the response of a resonator (or mode) with the use of an idler resonator (or mode), or to move energy between forced modes. Thus under the non-degenerate scheme it may be possible to move all the energy from one mode to another so that, despite being forced near resonance, that mode has no response.

Directions for future research suggested by this work include experimental validation of this non-degenerate vibration suppression technique. The parametrically amplified frequency sweeps in the single-input-single-output device discussed above also require experimental validation. To do this, it may also be necessary to explore alternative methods for introducing the parametric excitation since, as mentioned earlier, the application of parametric excitation to the input of the device does not efficiently accord with the modal contribution factors. In addition, the experiment presented in section 2.1 demonstrates limitations on achievable parametric amplification which do not agree with the theory presented. The reason is, as previously discussed, that the analysis assumes a linear system, and the experimental system will behave nonlinearly under large displacements. This suggests an investigation into the dynamic range of parametrically amplified devices including the limiting factors of both noise and nonlinearity. Noise properties in general warrant some inspection as the effect of noise on the parametric amplification-parametric resonance bifurcation boundary is not clearly understood. Furthermore, the phenomenon of stochastic resonance may have potential applications in MEMs sensors.

APPENDIX A

Multiple Scales Analysis

Consider the equation

$$M\ddot{x} + \epsilon C\dot{x} + K_1x + \epsilon K_2(t)x = \epsilon F(t)$$

where M, C, and K_1 are the $N \times N$ mass, damping, and stiffness matrices, respectively. $K_2(t)$ and F(t) are the periodic stiffness matrix and forcing vector. Let U be a matrix such that $U^TMU = I$ and $U^TK_1U = \Lambda$, where Λ is a diagonal matrix of the natural frequencies of the system. Now, we partially decouple the system with the change of coordinates x = Uy,

$$U^{T}MU\ddot{y} + \epsilon U^{T}CU\dot{y} + U^{T}K_{1}Uy + \epsilon U^{T}K_{2}Uy = \epsilon U^{T}F$$
$$\ddot{y}_{r} + \omega_{r}^{2}y_{r} = \epsilon \sum_{j=1}^{N} \left[-Z_{rj}\dot{y}_{j} - \Delta_{rj}y_{j} + U_{jr}F_{j} \right] \quad r = 1...N$$

where $Z=U^TCU$ and $\Delta=U^TK_2U$. Applying the method of multiple scales after [33], we make the substitutions

$$y_r = y_{r0}(T_0, T_1) + \epsilon y_{r1}(T_0, T_1) + O(\epsilon^2)$$
$$\dot{y}_r = D_0 y_{r0} + \epsilon D_1 y_{r0} + \epsilon D_0 y_{r1} + O(\epsilon^2)$$
$$\ddot{y}_r = D_0^2 y_{r0} + 2\epsilon D_0 D_1 y_{r0} + \epsilon D_0^2 y_{r1} + O(\epsilon^2)$$

where $T_0 = t$ and $T_1 = \epsilon t$. Then, we have

$$D_0^2 y_{r0} + 2\epsilon D_0 D_1 y_{r0} + \epsilon D_0^2 y_{r1} + \omega_r^2 y_{r0} + \epsilon \omega_r^2 y_{r1} = \epsilon \sum_{j=1}^{N} \left[-Z_{rj} \dot{y}_j - \Delta_{rj} y_j + U_{jr} F_j \right]$$

for r = 1...N. We now consider five different cases.

A.1 Case 1: Near an isolated primary resonance, $\Omega \approx \omega_k$

Here we take

$$\Delta_{rj} = \gamma_{rj} \cos(\Omega T_0 + \phi) + \delta_{rj} \cos(2\Omega T_0)$$

$$F_j = A_j \cos(\Omega T_0 + \phi) + B_j \cos(2\Omega T_0)$$

$$\Omega^2 = \omega_k^2 + \epsilon \sigma.$$

Then, for O(1), we have

$$D_0^2 y_{k0} + \Omega^2 y_{k0} = 0$$

$$D_0^2 y_{r0} + \omega_r^2 y_{r0} = 0 \quad r = 1...N \neq k$$

and thus

$$y_{k0} = Re \left\{ c_k(T_1)e^{i\Omega T_0} \right\}$$
$$y_{r0} = Re \left\{ c_r(T_1)e^{i\omega_r T_0} \right\}.$$

So, for $O(\epsilon)$, this gives

$$\begin{split} D_{0}^{2}y_{k1} &+ \Omega^{2}y_{k1} = \sigma c_{k}e^{i\Omega T_{0}} - 2i\Omega c_{k}'e^{i\Omega T_{0}} - \sum_{j=1}^{N} \left[i\omega_{j}Z_{kj}c_{j}e^{i\omega_{j}T_{0}} \right. \\ &+ \frac{1}{2}\gamma_{kj}c_{j} \left(e^{i(\omega_{j}+\Omega)T_{0}+\phi i} + e^{i(\omega_{j}-\Omega)T_{0}+\phi i} \right) \\ &+ \frac{1}{2}\delta_{kj}c_{j} \left(e^{i(\omega_{j}+2\Omega)T_{0}} + e^{i(\omega_{j}-2\Omega)T_{0}} \right) \\ &- U_{jk}A_{j}\cos(\Omega T_{0}+\phi) - U_{jk}B_{j}\cos(2\Omega T_{0}) \right] \\ D_{0}^{2}y_{r1} &+ \omega_{r}^{2}y_{r1} = -2i\omega_{r}c_{r}'e^{i\omega_{r}T_{0}} - \sum_{j=1}^{N} \left[i\omega_{j}Z_{rj}c_{j}e^{i\omega_{j}T_{0}} + \frac{1}{2}\gamma_{rj}c_{j} \left(e^{i(\omega_{j}+\Omega)T_{0}+\phi i} + e^{i(\omega_{j}-\Omega)T_{0}+\phi i} \right) \right. \\ &+ \frac{1}{2}\delta_{rj}c_{j} \left(e^{i(\omega_{j}+2\Omega)T_{0}} + e^{i(\omega_{j}-2\Omega)T_{0}} \right) \\ &- U_{jr}A_{j}\cos(\Omega T_{0}+\phi) - U_{jr}B_{j}\cos(2\Omega T_{0}) \right]. \end{split}$$

From these equations we can determine the frequency separation criteria. Here we see that we require that ω_k be distinct from all frequencies, that $|\omega_j \pm \omega_k| \neq |\omega_r|$, and that $|\omega_j \pm 2\omega_k| \neq |\omega_r|$ for $r,j=1...N \neq k$. Eliminating secular terms gives from the $O(\epsilon)$ equation gives

$$Re\left\{\sigma c_k e^{i\Omega T_0} - 2i\Omega c_k' e^{i\Omega T_0} - i\Omega Z_{kk} c_k e^{i\Omega T_0} + \frac{1}{2}\delta_{kk}c_k e^{-i\Omega T_0} - F_A \cos(\Omega T_0 + \phi)\right\} = 0$$

$$Re\left\{-2i\omega_r c + r' e^{i\omega_r T_0} - i\omega_r Z_{rr} c_r e^{i\omega_r T_0}\right\} = 0$$

where $F_A = \sum_{j=1}^N U_{jk} A_j$. Thus we have the slow-flow equations

$$\begin{bmatrix} X'_{k} \\ Y'_{k} \end{bmatrix} = \frac{1}{4\Omega} \begin{bmatrix} -2\Omega Z_{kk} & \delta_{kk} + 2\sigma \\ \delta_{kk} - 2\sigma & -2\Omega Z_{kk} \end{bmatrix} \begin{bmatrix} X_{k} \\ Y_{k} \end{bmatrix} + \begin{bmatrix} \frac{F_{A}\sin(\phi)}{2\Omega} \\ \frac{-F_{A}\cos(\phi)}{2\Omega} \end{bmatrix} \begin{bmatrix} X'_{r} \\ Y'_{r} \end{bmatrix} = \frac{1}{2} \begin{bmatrix} -Z_{rr} & 0 \\ 0 & -Z_{rr} \end{bmatrix} \begin{bmatrix} X_{r} \\ Y_{r} \end{bmatrix}$$

where $X_j = Re\{c_j\}$ and $Y_j = Im\{c_j\}$. Hence, $c_r \to 0$, and c_k has a fixed point

$$|c_{k}| = 2 \left[\left(F_{A}^{2} (\delta_{kk}^{2} + 4\Omega^{2} Z_{kk}^{2} - 4\Omega Z_{kk} \delta_{kk} \sin(2\phi) + 4\sigma^{2} + 4\sigma \delta_{kk} \cos(2\phi) \right) / (\delta_{kk}^{2} - 4(\sigma^{2} + \Omega^{2} Z_{kk}^{2}))^{2} \right]^{\frac{1}{2}}$$

$$\angle c_{k} = -\tan^{-1} \left(\frac{(\delta_{kk} - 2\sigma) \sin(\phi) - 2\Omega Z_{kk} \cos(\phi)}{(\delta_{kk} + 2\sigma) \cos(\phi) - 2\Omega Z_{kk} \sin(\phi)} \right)$$

$$G(\sigma = 0) = 2\Omega Z_{kk} \sqrt{\frac{\delta_{kk}^{2} + 4\Omega^{2} Z_{kk}^{2} - 4\Omega Z_{kk} \delta_{kk} \sin(2\phi)}{(\delta_{kk}^{2} - 4\Omega^{2} Z_{kk}^{2})^{2}}}.$$

This is stable for $\delta_{kk} \leq 2\sqrt{\sigma^2 + \Omega^2 Z_{kk}^2}$. Note that $\angle y_{k0} = -\angle c_k$.

A.2 Case 2: Near an isolated resonance of the sum type,

$$\Omega \approx \omega_p + \omega_q$$

Here we take

$$\Delta_{rj} = \delta_{rj} \cos(2\Omega T_0)$$

$$F_j = A_j \cos((2\Omega - \omega_p)T_0 + \theta) + B_j \cos(\omega_p T_0 + \psi) + C_j \cos(\Omega T_0 + \phi)$$

$$\Omega = \frac{\omega_p + \sqrt{\omega_q^2 + \epsilon \sigma}}{2}$$

$$\omega_q^2 = (2\Omega - \omega_p)^2 - \epsilon \sigma.$$

Thus, for O(1), we have

$$D_0^2 y_{p0} + \omega_p^2 y_{p0} = 0$$
$$D_0^2 y_{q0} + (2\Omega - \omega_p)^2 y_{q0} = 0$$

and

$$y_{p0} = Re \left\{ c_p(T_1) e^{i\omega_p T_0} \right\}$$
$$y_{q0} = Re \left\{ c_q(T_1) e^{i(2\Omega - \omega_p)T_0} \right\}.$$

So, for $O(\epsilon)$,

$$\begin{split} D_{0}^{2}y_{p1} &+ \omega_{p}^{2}y_{p1} = -2i\omega_{p}c_{p}'e^{i\omega_{p}T_{0}} - \sum_{j=1}^{N} \left[i\omega_{j}Z_{pj}c_{j}e^{i\omega_{j}T_{0}} \right. \\ &+ \frac{1}{2}\delta_{pj}c_{j} \left(e^{i(\omega_{j}+2\Omega)T_{0}} + e^{i(\omega_{j}-2\Omega)T_{0}} \right) - \\ &\left. U_{jp}(A_{j}\cos((2\Omega-\omega_{p})T_{0}+\theta) \right. \\ &\left. + B_{j}\cos(\omega_{p}T_{0}+\psi) + C_{j}\cos(\Omega T_{0}+\phi) \right) \right] \\ D_{0}^{2}y_{q1} &+ (2\Omega-\omega_{p})^{2}y_{q1} = \sigma c_{q}e^{i(2\Omega-\omega_{p})T_{0}} - \\ &\left. 2i(2\Omega-\omega_{p})c_{q}'e^{i(2\Omega-\omega_{p})T_{0}} \right. \\ &\left. - \sum_{j=1}^{N} \left[i\omega_{j}Z_{qj}c_{j}e^{i\omega_{j}T_{0}} + \frac{1}{2}\delta_{qj}c_{j} \left(e^{i(\omega_{j}+2\Omega)T_{0}} + e^{i(\omega_{j}-2\Omega)T_{0}} \right) \right. \\ &\left. - U_{jq}(A_{j}\cos((2\Omega-\omega_{p})T_{0}+\theta) + B_{j}\cos(\omega_{p}T_{0}+\psi) \right. \\ &\left. + C_{j}\cos(\Omega T_{0}+\phi) \right) \right]. \end{split}$$

Here we find the frequency conditions, $|\omega_j \pm 2\Omega| \neq |\omega_r|$, r, j = 1...N, except $2\Omega - \omega_q = \omega_p$. Also note that this frequency condition can exist simultaneously with that of case 1, and so we can have these two cases coexist without

coupling. Again, removing secular terms yields

$$Re \left\{ -2i\omega_p c_p' e^{i\omega_p T_0} - i\omega_p Z_{pp} c_p e^{i\omega_p T_0} - \frac{1}{2} \delta_{pq} c_q e^{-i\omega_p T_0} + F_B \cos(\omega_p T_0 + \psi) \right\} = 0$$

$$Re \left\{ \sigma c_q e^{i(2\Omega - \omega_p)T_0} - 2i(2\Omega - \omega_p) c_q' e^{i(2\Omega - \omega_p)T_0} - i(2\Omega - \omega_p) Z_{qq} c_q e^{i(2\Omega - \omega_p)T_0} - \frac{1}{2} \delta_{qp} c_p e^{-i(2\Omega - \omega_p)T_0} + F_A \cos((2\Omega - \omega_p)T_0 + \theta) \right\} = 0$$

where $F_A = \sum_{j=1}^N U_{jq} A_j$, and $F_B = \sum_{j=1}^N U_{jp} B_j$. Thus we have the slow-flow equations

$$X'_{q} = -\frac{1}{2}Z_{qq}X_{q} + \frac{\sigma}{2\omega_{q}}Y_{q} + \frac{\delta_{qp}}{4\omega_{q}}Y_{p} + \frac{F_{A}\sin(\theta)}{2\omega_{q}}$$

$$Y'_{q} = -\frac{\sigma}{2\omega_{q}}X_{q} - \frac{1}{2}Z_{qq}Y_{q} + \frac{\delta_{qp}}{4\omega_{q}}X_{p} - \frac{F_{A}\cos(\theta)}{2\omega_{q}}$$

$$X'_{p} = \frac{\delta_{pq}}{4\omega_{p}}Y_{q} - \frac{1}{2}Z_{pp}X_{p} + \frac{F_{B}\sin(\psi)}{2\omega_{p}}$$

$$Y'_{p} = \frac{\delta_{pq}}{4\omega_{p}}X_{q} - \frac{1}{2}Z_{pp}Y_{p} - \frac{F_{B}\cos(\psi)}{2\omega_{p}}$$

where $X_j=Re\{c_j\}$ and $Y_j=Im\{c_j\}$. This system has a fixed point where

$$|c_{q}| = 2\sqrt{\frac{F_{B}^{2}\delta_{qp}^{2} + 4F_{A}^{2}Z_{pp}^{2}\omega_{p}^{2} - 4F_{A}F_{B}Z_{pp}\delta_{qp}\omega_{p}\sin(\theta + \psi)}{16\sigma^{2}Z_{pp}^{2}\omega_{p}^{2} + (\delta_{pq}\delta_{qp} - 4Z_{pp}Z_{qq}\omega_{p}\omega_{q})^{2}}}$$

$$|c_{p}| = 2\left[\left(F_{A}^{2}\delta_{pq}^{2} + 4F_{B}^{2}(\sigma^{2} + Z_{qq}^{2}\omega_{q}^{2}) + 4F_{A}F_{B}\delta_{pq}(\sigma\cos(\theta + \psi) - Z_{qq}\omega_{q}\sin(\theta + \psi))\right)/(16\sigma^{2}Z_{pp}^{2}\omega_{p}^{2} + (\delta_{pq}\delta_{qp} - 4Z_{pp}Z_{qq}\omega_{p}\omega_{q})^{2})\right]^{\frac{1}{2}}.$$

This fixed point is stable for

$$\delta_{pq}\delta_{qp} < \frac{4\omega_{p}Z_{pp}Z_{qq}(\sigma^{2} + \omega_{q}^{2}(Z_{pp} + Z_{qq})^{2})}{\omega_{q}(Z_{pp} + Z_{qq})^{2}}.$$
62.

Thus, the combination resonance of the sum type can only be made unstable when δ_{pq} and δ_{qp} are of the same sign.

A.3 Case 3: Near an isolated resonance of the difference type, $\Omega pprox \omega_q - \omega_p$

This case results in the same solution as case 2 except with the change $\omega_p \to -\omega_p$ and $\psi \to -\psi$. Here, the stability condition becomes

$$\delta_{pq}\delta_{qp} > -\frac{4\omega_p Z_{pp} Z_{qq} (\sigma^2 + \omega_q^2 (Z_{pp} + Z_{qq})^2)}{\omega_q (Z_{pp} + Z_{qq})^2}.$$

Thus, the combination resonance of the difference type can only be made unstable when δ_{pq} and δ_{qp} are of different signs.

A.4 Case 4: Near $\omega_p + \omega_q$ and $\omega_s - \omega_q$

Let

$$\Delta_{rj} = \delta_{rj} \cos(\Omega T_0)$$

$$F_j = A_j \cos((\Omega - \omega_q) T_0 + \theta) + B_j \cos(\omega_q T_0 + \psi) +$$

$$C_j \cos((\Omega + \omega_q) T_0 + \phi)$$

$$\Omega = \omega_p + \omega_q + \epsilon \sigma_1 = \omega_s - \omega_q + \epsilon \sigma_2$$

$$\omega_p^2 \approx (\Omega - \omega_q)^2 - 2\epsilon(\Omega - \omega_q)\sigma_1$$

$$\omega_s^2 \approx (\Omega + \omega_q)^2 - 2\epsilon(\Omega + \omega_q)\sigma_2.$$

Thus, for O(1),

$$D_0^2 y_{p0} + (\Omega - \omega_q)^2 y_{p0} = 0$$

$$D_0^2 y_{q0} + \omega_q^2 y_{q0} = 0$$

$$D_0^2 y_{s0} + (\Omega + \omega_q)^2 y_{s0} = 0$$
63

and

$$y_{p0} = Re \left\{ c_p(T_1) e^{i(\Omega - \omega_q)T_0} \right\}$$

$$y_{q0} = Re \left\{ c_q(T_1) e^{i\omega_q T_0} \right\}$$

$$y_{s0} = Re \left\{ c_s(T_1) e^{i(\Omega + \omega_q)T_0} \right\}.$$

So, for $O(\epsilon)$,

$$\begin{split} D_{0}^{2}y_{p1} &+ (\Omega - \omega_{q})^{2}y_{p1} = 2(\Omega - \omega_{q})\sigma_{1}c_{p}e^{i(\Omega - \omega_{q})T_{0}} - \\ &- 2i(\Omega - \omega_{q})c'_{p}e^{i(\Omega - \omega_{q})T_{0}} \\ &- \sum_{j=1}^{N} \left[i\omega_{j}Z_{pj}c_{j}e^{i\omega_{j}T_{0}} + \frac{1}{2}\delta_{pj}c_{j}\left(e^{i(\omega_{j} + \Omega)T_{0}} + e^{i(\omega_{j} - \Omega)T_{0}}\right) \\ &- U_{jp}(A_{j}\cos((\Omega - \omega_{q})T_{0} + \theta) + B_{j}\cos(\omega_{q}T_{0} + \psi) \\ &+ C_{j}\cos((\Omega + \omega_{q})T_{0} + \phi)) \right] \\ D_{0}^{2}y_{q1} &+ \omega_{q}^{2}y_{q1} = -2i\omega_{q}c'_{q}e^{i\omega_{q}T_{0}} - \sum_{j=1}^{N} \left[i\omega_{j}Z_{qj}c_{j}e^{i\omega_{j}T_{0}} + \frac{1}{2}\delta_{qj}c_{j}\left(e^{i(\omega_{j} + \Omega)T_{0}} + e^{i(\omega_{j} - \Omega)T_{0}}\right) - \\ &- U_{jq}(A_{j}\cos((\Omega - \omega_{q})T_{0} + \theta) + B_{j}\cos(\omega_{q}T_{0} + \psi) \\ &+ C_{j}\cos((\Omega + \omega_{q})T_{0} + \phi)) \right] \\ D_{0}^{2}y_{s1} &+ (\Omega + \omega_{q})^{2}y_{s1} = 2(\Omega + \omega_{q})\sigma_{2}c_{s}e^{i(\Omega + \omega_{q})T_{0}} - \\ &- 2i(\Omega + \omega_{q})c'_{s}e^{i(\Omega + \omega_{q})T_{0}} \\ &- \sum_{j=1}^{N} \left[i\omega_{j}Z_{sj}c_{j}e^{i\omega_{j}T_{0}} + \frac{1}{2}\delta_{sj}c_{j}\left(e^{i(\omega_{j} + \Omega)T_{0}} + e^{i(\omega_{j} - \Omega)T_{0}}\right) - \\ &- U_{js}(A_{j}\cos((\Omega - \omega_{q})T_{0} + \theta) + B_{j}\cos(\omega_{q}T_{0} + \psi) \\ &+ C_{j}\cos((\Omega + \omega_{q})T_{0} + \phi)) \right]. \end{split}$$

Eliminating secular terms gives

$$Re \left\{ 2(\Omega - \omega_q)\sigma_1 c_p e^{i(\Omega - \omega_q)T_0} - 2i(\Omega - \omega_q)c_p' e^{i(\Omega - \omega_q)T_0} - i(\Omega - \omega_q)Z_{pp}c_p e^{i(\Omega - \omega_q)T_0} - \frac{1}{2}\delta_{pq}c_q e^{-i(\Omega - \omega_q)T_0} + F_A \cos((\Omega - \omega_q)T_0 + \theta) \right\} = 0$$

$$Re \left\{ -2i\omega_q c_q' e^{i\omega_q T_0} - i\omega_q Z_{qq}c_q e^{i\omega_q T_0} - \frac{1}{2}\delta_{qp}c_p e^{-i\omega_q T_0} - \frac{1}{2}\delta_{qs}c_s e^{i\omega_q T_0} + F_B \cos(\omega_q T_0 + \psi) \right\} = 0$$

$$Re \left\{ 2(\Omega + \omega_q)\sigma_2 c_s e^{i(\Omega + \omega_q)T_0} - 2i(\Omega + \omega_q)c_s' e^{i(\Omega + \omega_q)T_0} - i(\Omega + \omega_q)Z_{ss}c_s e^{i(\Omega + \omega_q)T_0} - \frac{1}{2}\delta_{sq}c_q e^{i(\Omega + \omega_q)T_0} + F_C \cos((\Omega + \omega_q)T_0 + \phi) \right\} = 0$$

which results in the slow flow equations

$$X'_{p} = -\frac{1}{2}Z_{pp}X_{p} + \sigma_{1}Y_{p} + \frac{\delta_{pq}}{4\omega_{p}}Y_{q} + \frac{F_{A}}{2\omega_{p}}\sin(\theta)$$

$$Y'_{p} = -\sigma_{1}X_{p} - \frac{1}{2}Z_{pp}Y_{p} + \frac{\delta_{pq}}{4\omega_{p}}X_{q} - \frac{F_{A}}{2\omega_{p}}\cos(\theta)$$

$$X'_{s} = -\frac{1}{2}Z_{ss}X_{s} + \sigma_{2}Y_{s} - \frac{\delta_{sq}}{4\omega_{s}}Y_{q} + \frac{F_{C}}{2\omega_{s}}\sin(\phi)$$

$$Y'_{s} = -\sigma_{2}X_{s} - \frac{1}{2}Z_{ss}Y_{s} + \frac{\delta_{sq}}{4\omega_{s}}X_{q} - \frac{F_{C}}{2\omega_{s}}\cos(\phi)$$

$$X'_{q} = \frac{\delta_{qp}}{4\omega_{q}}Y_{p} - \frac{\delta_{qs}}{4\omega_{q}}Y_{s} - \frac{1}{2}Z_{qq}X_{q} + \frac{F_{B}}{2\omega_{q}}\sin(\psi)$$

$$Y'_{q} = \frac{\delta_{qp}}{4\omega_{q}}X_{p} + \frac{\delta_{qs}}{4\omega_{q}}X_{s} - \frac{1}{2}Z_{qq}Y_{q} - \frac{F_{B}}{2\omega_{q}}\cos(\psi).$$

A.5 Case 5: Near $\omega_q - \omega_p$ and $\omega_s - \omega_q$

Let

$$\Delta_{rj} = \delta_{rj} \cos(\Omega T_0)$$

$$F_j = A_j \cos((\omega_q - \Omega)T_0 + \theta) + B_j \cos(\omega_q T_0 + \psi) + C_j \cos((\Omega + \omega_q)T_0 + \phi)$$

$$\Omega = \omega_q - \omega_p + \epsilon \sigma_1 = \omega_s - \omega_q + \epsilon \sigma_2$$

$$\omega_p^2 \approx (\omega_q - \Omega)^2 + 2\epsilon(\omega_q - \Omega)\sigma_1$$

$$\omega_s^2 \approx (\Omega + \omega_q)^2 - 2\epsilon(\Omega + \omega_q)\sigma_2.$$

Thus, for O(1),

$$D_0^2 y_{p0} + (\omega_q - \Omega)^2 y_{p0} = 0$$
$$D_0^2 y_{q0} + \omega_q^2 y_{q0} = 0$$
$$D_0^2 y_{s0} + (\Omega + \omega_q)^2 y_{s0} = 0$$

and

$$y_{p0} = Re \left\{ c_p(T_1) e^{i(\omega_q - \Omega)T_0} \right\}$$

$$y_{q0} = Re \left\{ c_q(T_1) e^{i\omega_q T_0} \right\}$$

$$y_{s0} = Re \left\{ c_s(T_1) e^{i(\Omega + \omega_q)T_0} \right\}.$$

So, for $O(\epsilon)$,

$$\begin{split} D_0^2 y_{p1} &+ (\omega_q - \Omega)^2 y_{p1} = -2(\omega_q - \Omega)\sigma_1 c_p e^{i(\omega_q - \Omega)T_0} - \\ &- 2i(\omega_q - \Omega)c_p' e^{i(\omega_q - \Omega)T_0} \\ &- \sum_{j=1}^N \left[i\omega_j Z_{pj} c_j e^{i\omega_j T_0} + \frac{1}{2} \delta_{pj} c_j \left(e^{i(\omega_j + \Omega)T_0} + e^{i(\omega_j - \Omega)T_0} \right) \right. \\ &- U_{jp} (A_j \cos((\omega_q - \Omega)T_0 + \theta) + B_j \cos(\omega_q T_0 + \psi) \\ &+ C_j \cos((\Omega + \omega_q)T_0 + \phi)) \right] \\ D_0^2 y_{q1} &+ \omega_q^2 y_{q1} = -2i\omega_q c_q' e^{i\omega_q T_0} - \sum_{j=1}^N \left[i\omega_j Z_{qj} c_j e^{i\omega_j T_0} + \right. \\ &\left. \frac{1}{2} \delta_{qj} c_j \left(e^{i(\omega_j + \Omega)T_0} + e^{i(\omega_j - \Omega)T_0} \right) - \right. \\ &\left. U_{jq} (A_j \cos((\omega_q - \Omega)T_0 + \theta) + B_j \cos(\omega_q T_0 + \psi) \right. \\ &+ C_j \cos((\Omega + \omega_q)T_0 + \phi)) \right] \\ D_0^2 y_{s1} &+ (\Omega + \omega_q)^2 y_{s1} = 2(\Omega + \omega_q)\sigma_2 c_s e^{i(\Omega + \omega_q)T_0} - \\ &\left. 2i(\Omega + \omega_q)c_s' e^{i(\Omega + \omega_q)T_0} \right. \\ &\left. - \sum_{j=1}^N \left[i\omega_j Z_{sj} c_j e^{i\omega_j T_0} + \frac{1}{2} \delta_{sj} c_j \left(e^{i(\omega_j + \Omega)T_0} + e^{i(\omega_j - \Omega)T_0} \right) \right. \\ &\left. - U_{js} (A_j \cos((\omega_q - \Omega)T_0 + \theta) + B_j \cos(\omega_q T_0 + \psi) \right. \\ &\left. + C_j \cos((\Omega + \omega_q)T_0 + \phi) \right) \right]. \end{split}$$

Eliminating secular terms gives

$$Re \left\{ -2(\omega_{q} - \Omega)\sigma_{1}c_{p}e^{i(\omega_{q} - \Omega)T_{0}} - 2i(\omega_{q} - \Omega)c'_{p}e^{i(\omega_{q} - \Omega)T_{0}} - i(\omega_{q} - \Omega)Z_{pp}c_{p}e^{i(\omega_{q} - \Omega)T_{0}} - \frac{1}{2}\delta_{pq}c_{q}e^{i(\omega_{q} - \Omega)T_{0}} + F_{A}\cos((\omega_{q} - \Omega)T_{0} + \theta) \right\} = 0$$

$$Re \left\{ -2i\omega_{q}c'_{q}e^{i\omega_{q}T_{0}} - i\omega_{q}Z_{qq}c_{q}e^{i\omega_{q}T_{0}} - \frac{1}{2}\delta_{qp}c_{p}e^{i\omega_{q}T_{0}} - \frac{1}{2}\delta_{qp}c_{p}e^{i\omega_{q}T_{0}} - \frac{1}{2}\delta_{qs}c_{s}e^{i\omega_{q}T_{0}} + F_{B}\cos(\omega_{q}T_{0} + \psi) \right\} = 0$$

$$Re \left\{ 2(\Omega + \omega_{q})\sigma_{2}c_{s}e^{i(\Omega + \omega_{q})T_{0}} - 2i(\Omega + \omega_{q})c'_{s}e^{i(\Omega + \omega_{q})T_{0}} - i(\Omega + \omega_{q})Z_{ss}c_{s}e^{i(\Omega + \omega_{q})T_{0}} - \frac{1}{2}\delta_{sq}c_{q}e^{i(\Omega + \omega_{q})T_{0}} + F_{C}\cos((\Omega + \omega_{q})T_{0} + \phi) \right\} = 0$$

which results in the slow flow equations

$$X'_{p} = -\frac{1}{2}Z_{pp}X_{p} - \sigma_{1}Y_{p} - \frac{\delta_{pq}}{4\omega_{p}}Y_{q} + \frac{F_{A}}{2\omega_{p}}\sin(\theta)$$

$$Y'_{p} = \sigma_{1}X_{p} - \frac{1}{2}Z_{pp}Y_{p} + \frac{\delta_{pq}}{4\omega_{p}}X_{q} - \frac{F_{A}}{2\omega_{p}}\cos(\theta)$$

$$X'_{s} = -\frac{1}{2}Z_{ss}X_{s} + \sigma_{2}Y_{s} - \frac{\delta_{sq}}{4\omega_{s}}Y_{q} + \frac{F_{C}}{2\omega_{s}}\sin(\phi)$$

$$Y'_{s} = -\sigma_{2}X_{s} - \frac{1}{2}Z_{ss}Y_{s} + \frac{\delta_{sq}}{4\omega_{s}}X_{q} - \frac{F_{C}}{2\omega_{s}}\cos(\phi)$$

$$X'_{q} = -\frac{\delta_{qp}}{4\omega_{q}}Y_{p} - \frac{\delta_{qs}}{4\omega_{q}}Y_{s} - \frac{1}{2}Z_{qq}X_{q} + \frac{F_{B}}{2\omega_{q}}\sin(\psi)$$

$$Y'_{q} = \frac{\delta_{qp}}{4\omega_{q}}X_{p} + \frac{\delta_{qs}}{4\omega_{q}}X_{s} - \frac{1}{2}Z_{qq}Y_{q} - \frac{F_{B}}{2\omega_{q}}\cos(\psi).$$

BIBLIOGRAPHY

- [1] J. F. Rhoads, N. J. Miller, S. W. Shaw, and B. F. Feeny, "Mechanical domain parametric amplification," Proceedings of ASME 2007 International Design Engineering Technical Conferences & Computers and Information in Engineering Conference, 2007.
- [2] B. E. DeMartini, J. F. Rhoads, S. W. Shaw, and K. L. Turner, "A single input-single output mass sensor based on a coupled array of microresonators," Sensors and Actuators A, vol. 137, 2007.
- [3] W. H. Louisell, Coupled Mode and Parametric Electronics. New York: John Wiley & Sons, Inc., 1960.
- [4] W. W. Mumford, "Some notes on the history of parametric transducers," *Preceedings of the IRE*, vol. 48, no. 5, pp. 848–853, 1960.
- [5] Howson and Smith, Parametric Amplifiers. London: McGraw-Hill, 1970.
- [6] D. W. Carr, "Fabrication, measurement, and analysis of nanomechanical structures in silicon," *Doctoral Dissertation Presented to the Faculty of the Graduate School of Cornell University*, 2000.
- [7] D. Rugar and P. Grütter, "Mechanical parametric amplification and thermomechanical noise squeezing," *Physical Review Letters*, vol. 67, no. 6, pp. 699-702, 1991.
- [8] R. Baskaran and K. L. Turner, "Mechanical domain coupled mode parametric resonance and amplification in a torsional mode micro electro mechanical oscillator," *Journal of Micromechanics and Microengineering*, vol. 13, pp. 701-707, 2003.
- [9] J. F. Rhoads, S. W. Shaw, K. L. Turner, J. Moehlis, B. E. DeMartini, and W. Zhang, "Generalized parametric resonance in electrostatically-actuated microelectromechanical oscillators," *Journal of Sound and Vibration*, vol. 296, no. 4-5, pp. 797–829, 2006.
- [10] E. F. W. Alexanderson, "A magnetic amplifier for radio telephony," *Preceedings of the IRE*, vol. 4, pp. 101–149, 1916.

- [11] C. M. Caves, "Quantum limits on noise in linear amplifiers," Physical Review D, vol. 26, no. 8, pp. 1817–1839, 1982.
- [12] J. Raskin, A. R. Brown, B. T. Khuri-Yakub, and G. M. Rebeiz, "A novel parametric-effect mems amplifier," *Journal of Microelectromechanical* Systems, vol. 9, no. 4, pp. 528-537, 2000.
- [13] S. M. Meerkov, "Principle of vibrational control: Theory and applications," IEEE Transactions on Automatic Control, vol. AC-25, no. 4, pp. 755–762, 1980.
- [14] E. K. P. P. T. Kabamba, S. M. Meerkov, "Pole placement capabilities of vibrational control," *IEEE Transactions on Automatic Control*, vol. 9, no. 43, pp. 1256–1261, 1998.
- [15] T. Ono, H. Wakamatsu, and M. Esashi, "Parametrically amplified thermal resonant sensor with pseudo-cooling effect," *Journal of MicroMechanics* and *Microengineering*, vol. 15, pp. 2282–2288, 2005.
- [16] G. D. Mansfeld, N. I. Polzikova, I. G. Prokhorova, and A. O. Raevskii, "Parametric effects in composite microwave bulk-acoustic-wave resonators," *Journal of Communications Technology and Electronics*, vol. 48, no. 7, pp. 791–798, 2003.
- [17] R. A. Baumgartner and R. L. Byer, "Optical parametric amplification," IEEE Journal of Quantum Electronics, vol. QE-15, no. 6, pp. 432-444, 1979.
- [18] B. Yurke, M. L. Roukes, R. Movshovich, and A. N. Pargellis, "A low-noise series-array josephson junction parametric amplifier," *Applied Physics Letters*, vol. 69, no. 20, pp. 3078–3080, 1996.
- [19] A. Olkhovets, D. W. Carr, J. M. Parpia, and H. G. Craighead, "Non-degenerate nanomechanical parametric amplifier," Micro Electro Mechanical Systems, the 14th IEEE International Conference on, pp. 298-300, 2001.
- [20] T. Ouisse, M. Stark, F. Rodrigues-Martins, S. H. B. Bercu, and J. Chevrier, "Theory of electric force microscopy in the parametric amplification regime," *Physical Review B*, vol. 71, 205404, 2005.
- [21] A. Dâna, F. Ho, and Y. Yamamoto, "Mechanical parametric amplification in piezoresistive gallium arsenide microcantilevers," *Applied Physics Letters*, vol. 72, no. 10, pp. 1152–1154, 1998.

- [22] I. Bargatin and M. L. Roukes, "Nanomechanical analog of a laser: Amplification of mechanical oscillations by stimulated zeeman transitions," Physical Review Letters, vol. 91(13), 138302(4), 2003.
- [23] V. Kaajakari and A. Lal, "Micromachined ultrasonic motor based on parametric polycrystalline silicon plate excitation," Sensors and Actuators A, vol. 137, pp. 120–128, 2007.
- [24] I. Bena, C. V. den Broeck, R. Kawai, M. Copelli, and K. Lindenberg, "Collective behavior of parametric oscillators," *Physical Review E*, vol. 65, 036611, 2002.
- [25] D. Goldobin and A. Pikovsky, "Collective modes in parametrically excited oscillator arrays," *Europhysics Letters*, vol. 59, no. 2, pp. 193–198, 2002.
- [26] Y. Bromberg, M. C. Cross, and R. Lifshitz, "Response of discrete nonlinear systems with many degrees of freedom," *Physical Review E*, vol. 73, 016214, 2006.
- [27] B. J. Gallacher, J. S. Burdess, A. J. Harris, and K. M. Harish, "Active damping control in mems using parametric pumping," NSTI-Nanotech, vol. 3, pp. 383–386, 2005.
- [28] M. Napoli, B. Bamieh, and K. Turner, "A capacitive microcantilever: Modelling, validation, and estimation using current measurements," *Journal of Dynamic Systems, Measurement, and Control*, vol. 126, pp. 319–326, 2004.
- [29] D. W. Carr, S. Evoy, L. Sekaric, H. G. Craighead, and J. M. Parpia, "Parametric amplification in a torsional microresonator," *Applied Physics Letters*, vol. 77, no. 10, pp. 1545–1547, 2000.
- [30] M. Requa and K. L. Turner, "Electromechanically driven and sensed parametric resonance in silicon microcantilevers," Applied Physics Letters, vol. 88, 263508, 2006.
- [31] M. Zalalutdinov, A. Olkhovets, A. Zehnder, B. Ilic, D. Czaplewski, H. G. Craighead, and J. M. Parpia, "Optically pumped parametric amplification for micromechanical oscillators," *Applied Physics Letters*, vol. 78, no. 20, pp. 3142-3144, 2001.
- [32] M. L. Roukes, K. L. Ekinci, Y. T. Yang, X. M. H. Huang, H. X. Tang, D. A. Harrington, J. Casey, and J. L. Arlett, "An apparatus and method for two-dimensional electron gas actuation and transductions for gas nems," *International Patent: Publication No: WO 2004/041998 A2*, 2004.

- [33] A. H. Nayfeh and D. T. Mook, Nonlinear Oscillations. New York: John Wiley & Sons, Inc., 1979.
- [34] J. M. Manley and H. E. Rowe, "Some general properties of nonlinear elements-part i. general energy relations," *Proceedings of the IRE*, vol. 44, no. 7, pp. 904-913, 1956.
- [35] J. F. Vignola, J. A. Judge, J. Jarzynski, M. Zalalutdinov, B. H. Houston, and J. W. Baldwin, "Effect of viscous loss on mechanical resonators designed for mass detection," *Applied Physics Letters*, vol. 88, 041921, 2006.
- [36] W. Zhang and K. L. Turner, "Frequency dependant fluid damping of micro and nano flexural resonators: Experiment, model and analysis," Sensors and Actuators A: Physical, vol. 134, pp. 594-599, 2007.
- [37] W. Zhang and K. L. Turner, "Pressure-dependent damping characteristics of micro silicon beam resonator for different resonant modes," IEEE Sensors 2005, Irvine, CA Oct 31st-Nov 3rd, 2005.
- [38] Y. T. Yang, C. Callegari, X. L. Feng, K. L. Ekinci, and M. L. Roukes, "Zeptogram-scale nanomechanical mass sensing," *Nano Letters*, vol. 6, no. 4, pp. 583-586, 2006.
- [39] T. P. Burg, A. R. Mirza, N. Milovic, C. H. Tsau, G. A. Popescu, J. S. Foster, and S. R. Manalis, "Vacuum-packaged suspended microchannel resonant mass sensor for biomolecular detection," *Journal of Microelectromechanical Systems*, vol. 15, no. 6, pp. 1466–1476, 2006.
- [40] J. Tamayo, A. D. L. Humphris, A. M. Malloy, and M. J. Miles, "Chemical sensors and biosensors in liquid environment based on microcantilevers with amplified quality factor," *Ultramicroscopy*, vol. 86, pp. 167-173, 2001.
- [41] J. Mertz, O. Marti, and J. Mlynek, "Regulation of a microcantilever response by force feedback," Applied Physics Letters, vol. 62, no. 19, pp. 2344-2346, 1993.
- [42] I. Dufour, S. M. Heinrich, and F. Josse, "Theoretical analysis of strong-axis bending mode vibrations for resonant microcantilever (bio)chemical sensors in gas or liquid phase," *Journal of Microelectromechanical Systems*, vol. 16, no. 1, pp. 44–49, 2007.

